The Quaternary calc-alkaline volcanism of the Patagonian Andes close to the Chile triple junction: geochemistry and petrogenesis of volcanic rocks from the Cay and Maca volcanoes (~45°S, Chile)

M. D'Orazio[a,b,*], F. Innocenti[a,b], P. Manetti[b,c], M. Tamponi[a], S. Tonarini[b], O. González-Ferrán[d], A. Lahsen[d], R. Omarini[e]

[a]*Dipartimento di Scienze della Terra, Università di Pisa, via S. Maria 53, I-56126 Pisa, Italy*
[b]*Istituto di Geoscienze e Georisorse, C.N.R., via Moruzzi 1, I-56124 Pisa, Italy*
[c]*Dipartimento di Scienze della Terra, Università di Firenze, via G. La Pira 4, I-50121 Firenze, Italy*
[d]*Departamento de Geología, Universidad de Chile, P.O. Box 13518, Santiago, Chile*
[e]*Departamento de Geología, Universidad Nacional de Salta, Buenos Aires 177, 4400 Salta, Argentina*

Abstract

Major- and trace-element, Sr–Nd isotopes, and mineral chemistry data were obtained for a collection of volcanic rock samples erupted by the Cay and Maca Quaternary volcanoes, Patagonian Andes (~45°S, Chile). Cay and Maca are two large, adjacent stratovolcanoes that rise from the Chiloe block at the southern end of the southern volcanic zone (SVZ) of the Andes. Samples from the two volcanoes are typical medium-K, calc-alkaline rocks that form two roughly continuous, largely overlapping series from subalkaline basalt to dacite. The overall geochemistry of the samples studied is very similar to that observed for most volcanoes from the southern SVZ. The narrow range of Sr–Nd isotope compositions ($^{87}Sr/^{86}Sr = 0.70389–0.70431$ and $^{143}Nd/^{144}Nd = 0.51277–0.51284$) and the major- and trace-element distributions indicate that the Cay and Maca magmas differentiated by crystal fractionation without significant contribution by crustal contamination. This is in accordance with the thin (< 30 km), relatively young (Paleozoic or more recent) continental crust beneath the volcanoes. The nature of the subduction-derived materials involved in the genesis of the Cay and Maca magmas is investigated by means of the relative concentration of fluid mobile (e.g. Ba) and fluid immobile (e.g. Nb, Ta, Zr, Y) elements and other relevant trace-element ratios (e.g. Sr/Y). The results indicate that small amounts (< 1 wt%) of both subducted sediments and slab-released fluids were added to the mantle sources of the Cay and Maca volcanoes and that, despite the very young age (< 10 Ma) of the oceanic lithosphere subducted beneath the volcanoes, slab melts were not involved in the magma genesis.

Notwithstanding the proximity of the Cay and Maca magma sources to the northern edge of the slab window generated by the subduction of the Chile ridge under the South American plate, we did not find any geochemical evidence for a contribution of a subslab asthenospheric mantle. However, this mantle has been used to explain the peculiar geochemical features (e.g. the mild alkalinity and relatively low ratios between large ion lithophile and high field strength elements) of the Hudson volcano, which is located even closer to the slab window than the Cay and Maca volcanoes are.

Keywords: Chile; Geochemistry; Geodynamics; Orogenic magmatism; Patagonian Andes; Petrology

1. Introduction

The Andean Cordillera is the most prominent effect of the subduction of oceanic lithosphere under the Pacific margin of South America. Since the Middle Miocene, two oceanic plates have been subducting beneath the South American plate: the Nazca plate to the north and the Antarctic plate to the south. These plates are separated by an active oceanic spreading ridge (Chile ridge) that is colliding, at an angle of approximately 20°, with the Chile trench near the Taitao Peninsula (46°12′S; Fig. 1).

The ridge–trench collision has been the cause of profound effects on the convergent margin configuration

* Corresponding author. Address: Dipartimento di Scienze della Terra, Università di Pisa, via S. Maria 53, I-56126 Pisa, Italy. Fax: +39-50-500932.
E-mail address: dorazio@dst.unipi.it (M. D'Orazio).

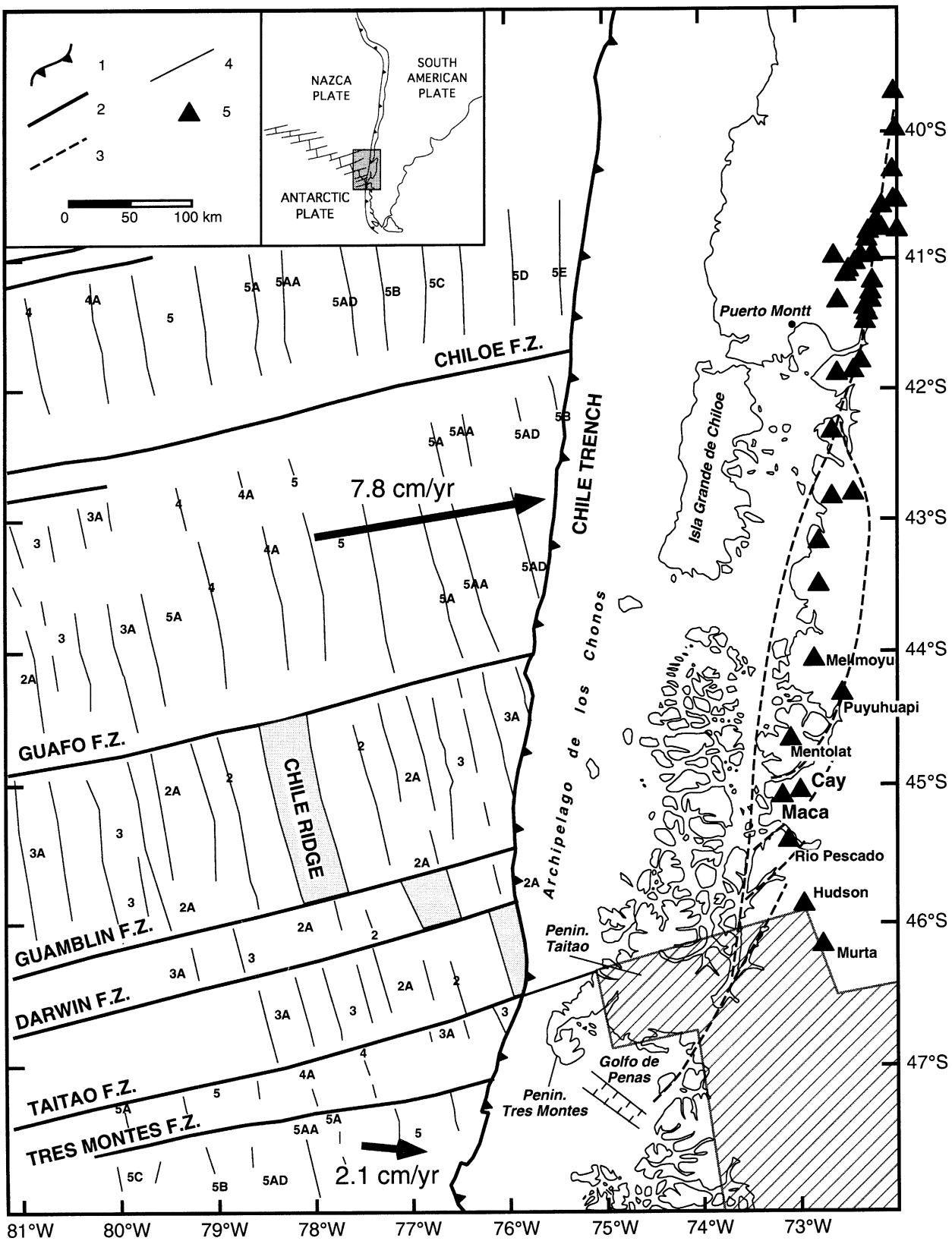

Fig. 1. Schematic geodynamic setting of the Pacific margin of southern South America between 39°S and 48°S (gray in inset). Legend: (1) Chile trench (teeth on overriding plate); (2) oceanic fracture zones; (3) main fault zones of the LOFS (Nelson et al., 1994); (4) oceanic magnetic anomalies (Tebbens et al., 1997); and (5) Plio–Quatenary cordilleran volcanoes. The stippled area indicates the vertical projection of the presumed slab window. The two large black arrows are the convergence vectors of the Nazca and Antarctic plates relative to the South American plate (according to the relative plate motion model NUVEL-1A; DeMets et al., 1994).

and the distribution and nature of the related magmatism (Herron et al., 1981; Forsythe and Nelson, 1985; Cande and Leslie, 1986; Bourgois et al., 1996). In particular, south of the Chile Triple Junction (CTJ), where the Nazca, Antarctic, and South American plates meet, the Cordillera loses its continuity, and there is a 350 km long volcanic gap (Ramos and Kay, 1992). A slab window opening southeast of the CTJ (Murdie and Russo, 1999) caused the cessation of calc-alkaline volcanism along the Cordillera and promoted the formation of widespread basaltic plateaus, with a prevailing intraplate geochemical signature, in extra-Andean Patagonia (Ramos and Kay, 1992; Gorring et al., 1997; D'Orazio et al., 2000, 2001; Gorring and Kay, 2001). The complexity of the magmatism in this sector of the Pacific margin of southern South America is also shown by the bimodal magmatism of MORB-type products, occurring along with acidic calc-alkaline magmas, found in the forearc region close to the CTJ (Guivel et al., 1999; Lagabrielle et al., 2000).

The discontinuity in the subducting lithosphere due to ridge subduction should have had some unascertained effects on the calc-alkaline magmatism of the Cordillera close to the discontinuity. We present new petrographic and geochemical data on two central volcanoes of the southernmost Andes: Cay and Maca. These volcanoes, along with the Hudson volcano, are the Andean central volcanoes closest to the CTJ (Fig. 1). We use major- and trace-element distributions and Sr–Nd isotopes to investigate the low-pressure processes that cause inter- and intra-volcano geochemical variability, the nature of the slab-derived components that metasomatize the wedge mantle, and the possible geochemical effects related to the proximity of the mantle sources to the discontinuity in the subducting slab.

2. Geological background

The southern volcanic zone (SVZ) of the Andean Cordillera is the segment of the chain between 33°S and 46°S. Calc-alkaline volcanics from the SVZ are mainly high Al_2O_3 basalts and basaltic andesites, whereas more evolved rock types characterize the central volcanic zone (CVZ; 16°S–28°S). In addition, the SVZ is founded on a thin Paleozoic, or younger, crust, whereas a thick Precambrian–Paleozoic basement occurs beneath the CVZ. To the south, the SVZ is separated from the Austral volcanic zone (AVZ; 49°S–54°S) by a ~350 km long volcanic gap. The AVZ is formed by six active stratovolcanoes (Lautaro, Viedma, Aguilera, Reclus, Burney, and Cook) that erupted magmas with an 'adakitic' signature (Stern and Kilian, 1996; Sigmarsson et al., 1998).

Futa and Stern (1988) introduce a further subdivision of the SVZ into the northern SVZ (NSVZ; 33°S–37°S) and southern SVZ (SSVZ; 37°S–46°S). At the SSVZ latitudes, the thickness of the continental crust is less than 30 km, and the age of the oceanic crust of the Nuzca plate entering the Chile trench is less than 33 Ma (Herron et al., 1981). Moreover, the volcanoes of the SSVZ lie west of the axis of the Cordillera Principal and have basal elevations of less than 1000 m.

Along the segment of the SSVZ between 44°S and 46°S, there is a series of five large stratovolcanoes (from north to south: Melimoyu, Mentolat, Cay, Maca, and Hudson) (Fig. 1). These volcanoes have spacings of 15–100 km and are associated with volcanic fields made up of small, monogenetic scoria cones and associated basaltic lavas (Puyuhuapi, Río Pescado, Río Murta; Lahsen et al., 1994, 1997; González-Ferrán et al., 1996; Demant et al., 1998). The geologic evolution of this segment of the Cordillera is closely connected to the activity of the Liquiñe–Ofqui dextral transcurrent fault system (LOFS). According to most authors (Nelson et al., 1994; Cembrano et al., 1996), this system originated in response to the oblique subduction of the Nazca plate beneath the South American continent. Transcurrent movements since the Late Miocene have formed a continental forearc sliver, the Chiloe block, that moves northward with respect to the South American plate. The movement of the Chiloe block is accommodated by normal faulting in the Golfo de Penas basin and right-lateral strike-slip and dip-slip displacements along the LOFS (Nelson et al., 1994). The relationships between the LOFS and volcanic activity are clear, as shown by the monogenetic cones. These are aligned along the main faults of the LOFS, as can be observed for the eruptive centers of Puyuhuapi and Río Pescado. The age at the latitude of 44°S–46°S varies from 6 to 5 Ma to the north to 0 Ma at the CTJ (Fig. 1).

The Quaternary volcanic structures located in this sector (44°S–46°S) grew above a basement composed of either Meso-Cenozoic intrusive rocks (mainly granodiorites and tonalites) of the North Patagonian batholith (Hervé et al., 1993; Parada et al., 2000) or Cenozoic, low- to medium-grade metamorphic rocks (Hervé et al., 1995).

The geological investigation of these stratovolcanoes is still in its initial stages because of their limited accessibility (i.e. absence of roads, dense vegetation, large glaciers, high precipitation). The Hudson volcano is an exception because in 1971 and August 1991, it gave rise to two plinian eruptions whose products have been the objects of several detailed volcanological and geochemical studies (Déruelle and Bourgois, 1993; Naranjo and Stern, 1998).

3. Cay and Maca volcanoes: extent of knowledge

The Maca (45°05.5′S, 73°10.5′W) and Cay (45°02.8′S, 72°59.3′W) stratovolcanoes rise approximately 15 km apart in the central portion of the region between the Puyuhuapi and Aysén fiords. They lie ~230 km east of the Chile trench (Fig. 1) at the intersection of NE–SW- and NW–SE-trending faults that belong to the LOFS (Fig. 2).

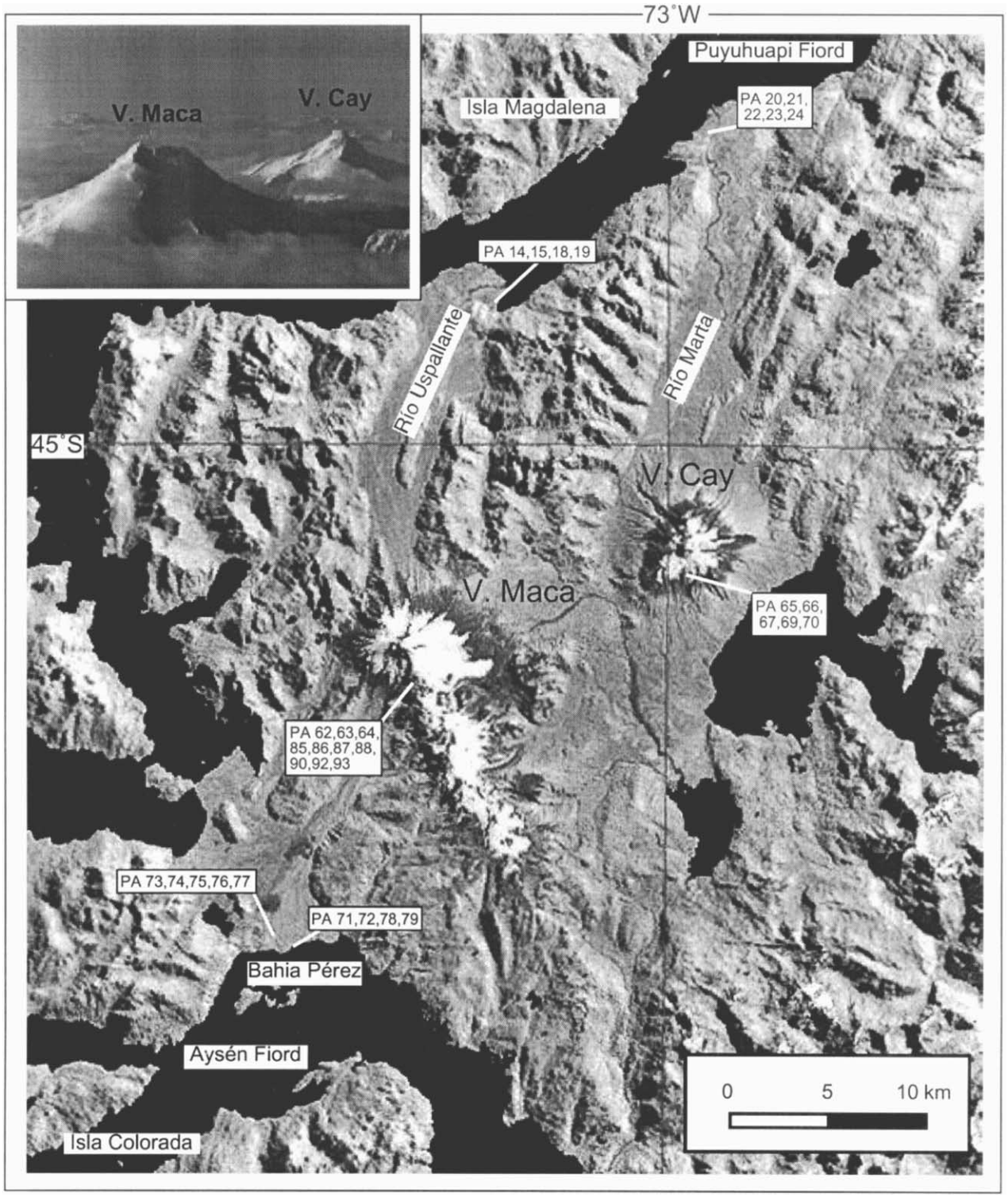

Fig. 2. Landsat 5 MSS image (March 7, 1985, path/row 232/091) of the Cay and Maca volcanic areas. The morphostructural setting is clearly controlled by NE–SW and NW–SE fractures related to the LOFS. Inset: panoramic view of the Maya and Cay volcanoes taken from the SSW. The approximate locations of the studied samples are also reported.

The Maca volcano occurs at the NW end of a prominent, NW–SE-trending volcanic ridge, ~10 km long by ~3 km wide. This ridge has an elevation of 1500–1700 m. The summit area of the volcano (maximum elevation 2960 m) presents a steep-sided depression opening toward the SSE, probably due to a flank failure. Parasitic cones, aligned along a NE–SW trend, occur at low elevations (down to the sea level), particularly on the SW flank of the volcano (González-Ferrán, 1994), as far as the northern shore of the Aysén fiord (Bahia Pérez) and in the middle of the fiord

itself, close to its entrance (Isla Colorada; Fig. 2). Some cones have produced small subaerial lava flows with well-preserved morphology and thin vegetation cover. The southernmost cones, as indicated by the presence of hyaloclastitic products, were produced by subaqueous activity (Demant et al., 1994).

The Cay volcano is an isolated conical structure culminating at 2200 m. A series of parasitic cones is distributed below 1000 m along a NE–SW direction on the SW flank of the volcano.

Volcanic rocks analyzed for this study were sampled from five distinct areas (Fig. 2). The Maca samples were collected at the mouth of the Río Uspallante (northern sector of the volcano) and on the southern slope of the cone between 1350 and 1400 m (helicopter-assisted sampling); the volcanic products erupted by the parasitic cones of Maca were collected in the Bahia Pérez area (northern Aysén fiord). Cay lavas were sampled in the northern sector, at the mouth of the Río Marta, and on the southern slope of the volcanic structure (~1000 m, helicopter-assisted sampling).

4. Classification and petrographic summary

The volcanic rocks of this study are subalkaline and belong to a calc-alkaline series (Fig. 3; Miyashiro, 1974). In the K_2O–SiO_2 classification diagram (Peccerillo and Taylor, 1976), they fall within the basalt, basaltic andesite, andesite, and dacite fields (Fig. 4). Basalts fall close to

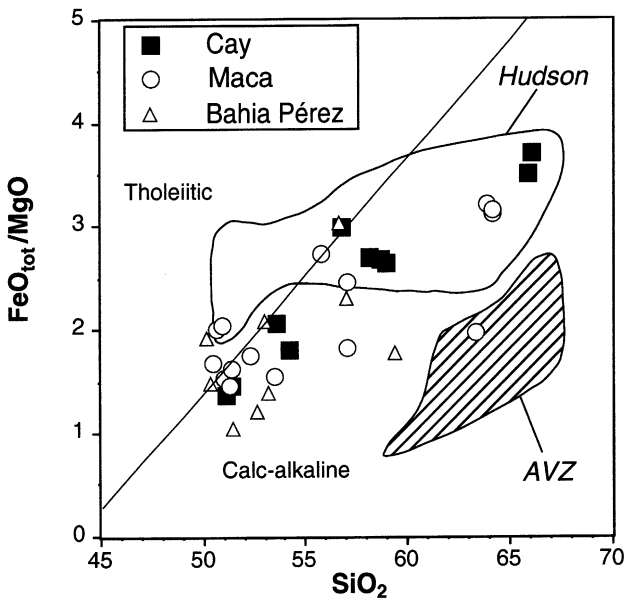

Fig. 3. FeO_{tot}/MgO versus SiO_2 (wt%) diagram for discriminating tholeiitic from calc-alkaline rocks (Miyashiro, 1974). FeO_{tot} is total iron calculated as FeO. The fields for the Hudson volcano (López-Escobar et al., 1993; Naranjo and Stern, 1998) and for the AVZ volcanoes (Futa and Stern, 1988; Stern and Kilian, 1996) are shown for comparison. In this diagram and in Figs. 4, 7, and 12, analyses were recalculated to 100 wt%, LOI free, before plotting.

the boundary with the low-K series. In the K_2O–SiO_2 diagram, the volcanic rocks from the Hudson volcano define a trend characterized by significantly higher K_2O levels, cutting across the boundary between the medium- and high-K series (Fig. 4). In the total alkali-silica diagram (not shown), the Hudson volcanics fall in the alkaline field close to the alkaline/subalkaline boundary. An apparent gap in silica content is observed between 59 and 63 wt% (Fig. 4). This gap could be attributed to either an incomplete sampling or a bimodal distribution of the erupted products.

Overall, rocks from the Cay and Maca volcanic regions do not show significantly distinct petrographical features, so we describe their petrography collectively. The relative abundance of the different rock types in our sample collection conforms the general predominance of basalts and basaltic andesites over differentiated volcanics observed in the SVZ of the Andes (Futa and Stern, 1988). Study samples are porphyritic/glomeroporphyritic rocks (5–35 vol%) with phenocryst assemblages made up of anhydrous minerals (plagioclase, olivine, augite, orthopyroxene, Ti-magnetite). Selected analyses of the main phases are presented in Tables 1–4.

Basalts are moderately to highly porphyritic rocks with a prevailing phenocryst assemblage of plagioclase + olivine. Plagioclase is the dominant phenocryst phase and reaches a maximum length of 3–4 mm (avg. 1.5–2 mm). Normal and oscillatory zoning and sieve-textured cores are common. The composition is largely variable (Fig. 5) from bytownite cores (An_{70-89}) to labradorite rims (~An_{55}). Olivine phenocrysts are smaller than plagioclases, with most frequent sizes of 0.4–0.6 mm (max 1 mm). The largest crystals are sometimes rounded and/or embayed. Usually, olivine is zoned with Mg-rich cores (up to Fo_{84}) and more iron-rich rims (up to Fo_{60}). Minor clinopyroxene phenocrysts, augitic in composition (Fig. 6), appear in some samples. Glomerophyric aggregates of olivine + plagioclase ± augite ± Ti-magnetite are sporadic. Plagioclase, augite, and Ti-magnetite constitute the groundmass of basalts with minor quantities of interstitial glass. However, very different petrographical features characterize a single basaltic sample from Bahia Pérez (PA-71). This sample is olivine–phyric with reasonably large (~1–1.5 mm), poorly zoned, Mg-rich (Fo_{87-84}) phenocrysts rich in Cr-spinel inclusions.

Basaltic andesites and andesites are porphyritic rocks with moderate to low phenocryst content. Phenocryst assemblages are composed of plagioclase, olivine, clinopyroxene, orthopyroxene, and Ti-magnetite. The main petrographic difference between basalts and basaltic andesites + andesites is the higher abundance of pyroxene phenocrysts and more frequent presence of Ti-magnetite microphenocrysts in the latter. The proportion of olivine phenocrysts decreases from the less evolved basaltic andesites to the more evolved andesites, in which they are missing. In some cases, olivine phenocrysts/microphenocrysts are strongly embayed and rimmed by subcalcic

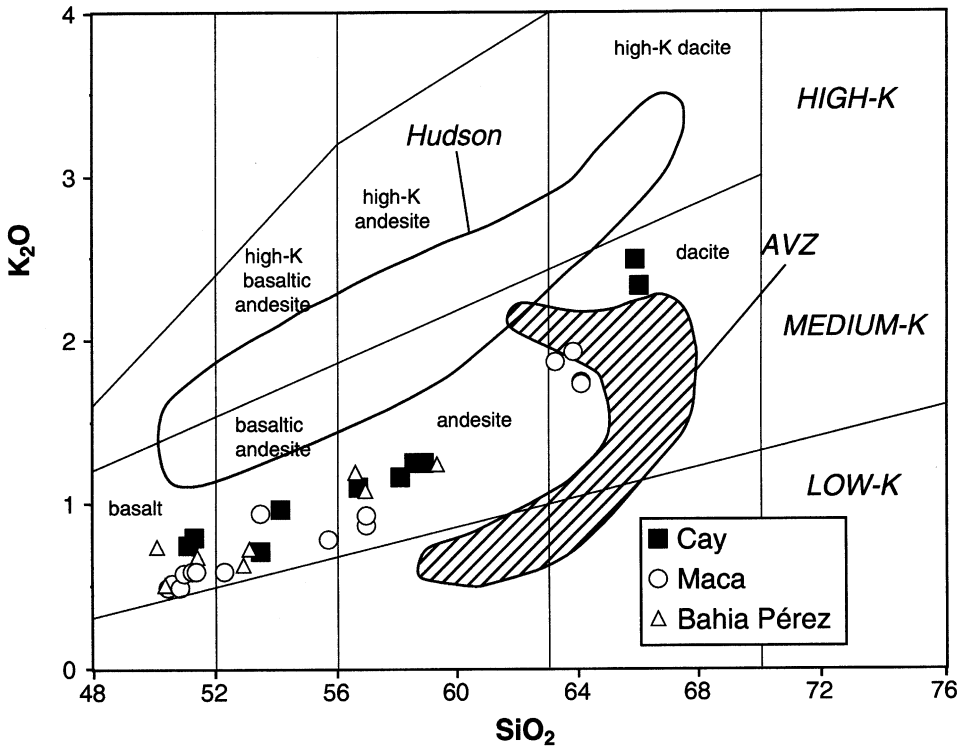

Fig. 4. K_2O versus SiO_2 (wt%) classification diagram (Peccerillo and Taylor, 1976).

clinopyroxene (Fig. 6). Plagioclase, augite, and Ti-magnetite are frequently joined to form glomerophyric aggregates. The groundmass is made up of plagioclase, augite, Ca-poor pyroxene, Ti-magnetite, and abundant brownish glass.

Dacite samples are low porphyricity rocks. Phenocrysts are mainly clear, euhedral, andesinic–labradoritic plagioclase (Fig. 5) with minor orthopyroxene, augite, Ti-magnetite, apatite, and rare corroded olivine. In sample PA-24 (Cay), rare phenocrysts of brown amphibole rimmed by opaques are also found. The groundmass is made up of strongly oriented plagioclase microlites, augite, pigeonite, Ti-magnetite, and abundant brown glass. Groundmass textures vary from almost glassy to hyalopilitic.

In summary, the calc-alkaline volcanic rocks from the Maca and Cay areas are characterized by several peculiar petrographic features: (1) an almost complete absence of hydrous silicate phases; (2) an An-rich composition of plagioclase in all samples (including dacites); (3) the persistence of olivine phenocrysts (even with evidence of disequilibrium) in medium-differentiated lavas; (4) a lack of quartz in the dacite samples; and (5) a decrease in phenocryst content with evolution.

5. Geochemistry

5.1. Major elements

Major- and trace-element analyses of volcanic rocks from the Maca and Cay volcanoes and the parasitic cones of Bahia Pérez are reported in Table 5. In Harker's diagrams (Fig. 7), the samples from the three volcanic occurrences define largely overlapping variation trends, indicating a first-order consanguinity of the products erupted by these volcanoes. From basalts to dacites, we observe a decrease of CaO, MgO, FeO_{tot}, and Al_2O_3 and an increase of K_2O and Na_2O. The variation of TiO_2 and P_2O_5 concentrations across the data set is marked by an increase in the basic and intermediate rock interval (60–63 wt% SiO_2) and rapid decrease in the most evolved compositions (Fig. 7). The behavior of these two elements indicates that apatite and Ti-magnetite were major fractionating phases when the evolving magma reached ~60–62 wt% SiO_2. Basalts and basaltic andesites show a high dispersion of the data points, particularly for Al_2O_3, FeO_{tot}, and MgO, probably due to cumulus fractionation of the plagioclases plus mafic minerals. In Harker's diagrams (Fig. 7), the volcanic rocks from the Hudson volcano define variation trends that largely overlap with those of the Cay and Maca volcanoes, but some systematic differences are observed: (1) at a given SiO_2 content, Hudson volcanics have more Na_2O and K_2O and less CaO and MgO and show higher K_2O/Na_2O ratios (Figs. 4 and 7); (2) basaltic rocks from the Hudson volcano are richer in TiO_2, FeO_{tot}, and P_2O_5; and (3) the Al_2O_3 content of the Hudson volcanics is less variable (~15–17 wt%).

In summary, major-element variations in the study samples suggest that they form a comagmatic series and that the major process controlling their differentiation was crystal fractionation of solid assemblages made of

Table 1
Selected analyses of olivine

	Cay														
Method	EMP	EMP	SEM-EDS	SEM-EDS	EMP	SEM-EDS	SEM-EDS	SEM-EDS	SEM-EDS	SEM-EDS	SEM-EDS	SEM-EDS	SEM-EDS	SEM-EDS	SEM-EDS
Sample	PA-23 ph. core	PA-23 ph. core	PA-23 ph. rim	PA-23 ph. core	PA-23 ph. core	PA-23 grm	PA-67 ph. core	PA-67 ph. rim	PA-67 ph. core	PA-67 ph. rim	PA-65 ph. core	PA-65 ph. core	PA-65 ph. rim	PA-65 ph. core	PA-65 ph. rim
SiO_2	38.38	39.58	35.80	38.97	38.27	36.28	38.17	37.23	37.45	36.64	36.58	37.00	36.51	37.32	36.24
FeO	23.14	15.90	32.81	22.66	25.42	36.88	25.68	29.90	28.86	32.63	30.20	28.43	32.71	28.13	33.70
MnO	0.59	0.30	0.67	0.37	0.62	0.66	0.59	0.68	0.51	0.64	0.94	0.78	1.08	0.48	0.80
MgO	38.91	45.38	30.37	38.00	35.55	26.18	35.56	32.18	33.18	30.08	32.13	33.62	29.53	34.07	29.26
CaO	0.26	0.17	0.35	<d.l.	<d.l.	<d.l.	<d.l.	<d.l.	<d.l.	<d.l.	0.15	0.17	0.17	<d.l.	<d.l.
Total	101.28	101.33	100.00	100.00	99.86	100.00	100.00	100.00	100.00	100.00	100.00	100.00	100.00	100.00	100.00
Fo%	75.0	83.6	62.3	74.9	71.4	55.9	71.2	65.7	67.2	62.2	65.5	67.8	61.7	68.3	60.8
z	Maca											Bahia Pérez			
Method	EMP	EMP	SEM-EDS	EMP	EMP	EMP	EMP	EMP	EMP	SEM-EDS	EMP	SEM-EDS	SEM-EDS	SEM-EDS	EMP
Sample	PA-19 ph. core	PA-19 ph. rim	PA-19 grm	PA-15 ph. core	PA-15 ph. rim	PA-15 grm	PA-93 μph.	PA-93 ph. core	PA-93 ph. rim	PA-93 grm	PA-93 grm	PA-71 ph. core	PA-71 ph. rim	PA-71 ph. core	PA-71 ph. rim
SiO_2	38.11	37.07	38.18	37.80	37.94	37.68	37.58	37.02	36.50	37.97	34.06	40.71	40.46	40.84	40.00
FeO	20.26	28.38	28.06	25.25	24.44	29.17	20.23	31.71	32.79	27.80	40.11	12.26	13.89	12.52	14.34
MnO	0.44	0.60	0.48	0.49	0.44	0.55	0.40	0.46	0.64	0.78	1.06	0.26	0.16	0.18	<d.l.
MgO	42.28	35.46	33.28	37.63	38.21	32.48	41.02	32.01	31.59	33.45	24.64	46.63	45.33	46.32	44.85
CaO	0.21	0.27	<d.l.	0.23	0.24	<d.l.	0.28	0.27	0.28	<d.l.	<d.l.	0.14	0.16	0.14	0.13
Total	101.30	101.78	100.00	101.40	101.27	99.88	99.51	101.47	101.80	100.00	99.87	100.00	100.00	100.00	99.32
Fo%	78.8	69.0	67.9	72.7	73.6	66.5	78.3	64.3	63.2	68.2	52.3	87.1	85.3	86.8	84.8

Notes for Tables 1–4: pH = phenocryst; μph: = microphenocryst; grm = groundmass; ≤ d.l. = below detection limit. EMP = electron microprobe; SEM-EDS: scanning electron microscope-energy dispersive spectrometer. The 100.0% closure of the SEM-EDS analyses are imposed by the EDAX DX4 data reduction.

Table 2
Selected analyses of pyroxene

	Cay														
Method	EMP	EMP	EMP	EMP	SEM-EDS	SEM-EDS	SEM-EDS	SEM-EDS	SEM-EDS	EMP	EMP	EMP	EMP	EMP	EMP
Sample	PA-23 ph. core	PA-23 ph. rim	PA-23 ph. core	PA-23 ph. rim	PA-67 ph. core	PA-67 ph. rim	PA-67 grm	PA-65 ph. core	PA-65 ph. rim	PA-21 μph.	PA-21 μph.	PA-21 μph.	PA-21 μph.	PA-21 ph. core	PA-21 ph. rim
SiO_2	51.11	49.99	50.86	50.50	52.58	51.17	53.47	50.13	49.40	51.36	52.58	52.48	52.65	51.46	50.91
TiO_2	0.48	1.06	0.82	0.90	0.24	0.64	0.31	1.04	0.97	0.52	0.27	0.28	0.34	0.65	0.67
Al_2O_3	1.68	3.87	2.93	2.99	1.41	3.00	0.74	3.27	4.46	1.61	0.88	0.70	1.08	1.99	1.92
Cr_2O_3	0.20	0.44	0.26	<d.l.	<d.l.	0.19	<d.l.	<d.l.	<d.l.	<d.l.	<d.l.	<d.l.	<d.l.	<d.l.	<d.l.
FeO_{tot}	8.79	8.50	9.22	10.44	9.09	9.15	18.78	9.29	9.57	10.36	21.35	21.33	20.64	10.53	10.82
MnO	0.36	0.29	0.32	0.47	0.70	0.47	0.65	0.40	0.57	0.48	1.08	1.07	1.10	0.60	0.70
MgO	17.41	15.15	16.13	15.35	15.34	15.80	21.80	14.74	14.21	14.54	23.05	22.62	22.70	14.70	14.39
CaO	18.26	20.00	19.02	18.86	20.23	19.18	3.95	20.50	20.24	20.09	1.53	1.77	2.13	19.57	19.78
Na_2O	0.21	0.31	0.37	0.32	0.41	0.40	0.30	0.63	0.58	0.43	<d.l.	<d.l.	<d.l.	0.29	0.30
Total	98.50	99.61	99.93	99.83	100.00	100.00	100.00	100.00	100.00	99.39	100.74	100.25	100.64	99.79	99.49
Wo%	37.1	41.7	38.9	38.7	41.1	39.4	8.0	42.3	42.2	41.3	3.0	3.5	4.2	40.2	40.6
En%	49.3	44.0	45.9	43.8	43.4	45.2	61.3	42.3	41.3	41.6	63.5	62.8	62.7	42.0	41.1
Fs%	13.6	14.3	15.2	17.5	15.5	15.4	30.7	15.4	16.5	17.1	33.4	33.7	33.1	17.8	18.3
	Maca														
Method	SEM-EDS	SEM-EDS	SEM-EDS	SEM-EDS	SEM-EDS	SEM-EDS	SEM-EDS	SEM-EDS	SEM-EDS	SEM-EDS	SEM-EDS	SEM-EDS	SEM-EDS	SEM-EDS	SEM-EDS
Sample	PA-19 grm	PA-19 grm	PA-19 grm	PA-15 grm	PA-15 grm	PA-93 grm	PA-93 grm	PA-93 grm	PA-85 ph. core	PA-85 ph. rim	PA-90 ph. core	PA-90 grm	PA-90 grm	PA-90 ph. core	PA-90 ph. core
SiO_2	50.33	50.31	49.99	48.47	50.91	51.76	51.83	50.41	51.07	51.17	53.81	52.04	50.80	50.57	53.07
TiO_2	1.06	0.87	0.94	1.41	0.75	0.57	0.43	0.90	0.85	0.67	0.51	0.54	0.48	0.56	0.22
Al_2O_3	3.53	3.14	3.39	3.49	1.90	2.03	2.02	2.28	2.69	2.93	1.10	1.62	1.47	2.31	1.08
Cr_2O_3	0.13	0.75	0.19	<d.l.	<d.l.	0.20	0.23	0.32	0.25	<d.l.	0.10	<d.l.	<d.l.	0.13	<d.l.
FeO_{tot}	11.17	10.16	10.50	13.80	12.61	9.68	9.91	10.30	9.53	9.34	16.86	23.10	23.18	9.60	17.83
MnO	0.33	0.40	0.21	0.49	0.18	0.39	0.42	0.50	0.61	0.50	1.00	1.47	1.49	0.63	0.91
MgO	16.38	17.17	16.73	13.61	14.51	16.57	16.87	15.58	15.13	15.19	24.39	16.69	16.72	14.65	24.71
CaO	16.46	16.49	17.35	18.03	18.79	18.17	17.72	19.01	19.33	19.47	1.74	4.16	5.42	21.02	1.54
Na_2O	0.61	0.71	0.70	0.70	0.35	0.63	0.57	0.70	0.54	0.73	0.49	0.38	0.44	0.53	0.64
Total	100.00	100.00	100.00	100.00	100.00	100.00	100.00	100.00	100.00	100.00	100.00	100.00	100.00	100.00	100.00
Wo%	34.1	34.1	35.7	38.0	38.6	37.1	36.0	39.4	40.0	40.3	3.5	8.9	11.3	43.0	3.1
En%	47.3	49.5	47.8	39.9	41.5	47.1	47.7	44.9	43.6	43.8	68.4	49.9	48.5	41.7	68.8
Fs%	18.6	16.4	16.5	22.1	20.0	15.8	16.2	15.7	16.4	15.9	28.1	41.2	40.1	15.2	28.1

Table 3
Selected analyses of feldspars

	Cay														
Method	SEM-EDS	EMP	SEM-EDS	SEM-EDS	SEM-EDS	SEM-EDS	SEM-EDS	SEM-EDS	SEM-EDS	SEM-EDS	SEM-EDS	SEM-EDS	SEM-EDS	EMP	EMP
Sample	PA-23 ph. core	PA-23 ph. core	PA-23 μph.	PA-23 μph.	PA-67 ph. core	PA-67 ph. core	PA-67 ph. rim	PA-67 μph.	PA-67 grm	PA-65 ph. core	PA-65 ph. rim	PA-65 ph. core	PA-65 grm	PA-21 ph. core	PA-21 ph. rim
SiO_2	47.92	50.02	53.01	52.02	46.41	46.47	50.33	52.48	53.66	46.75	51.75	47.68	52.55	54.73	55.55
Al_2O_3	33.16	30.67	28.74	29.36	34.44	34.22	31.39	29.85	29.39	33.65	30.30	33.32	30.00	28.55	28.43
Fe_2O_3	0.69	1.01	1.10	0.94	0.48	0.48	0.83	0.70	0.75	0.77	0.60	0.51	0.56	0.62	0.52
CaO	16.35	13.77	12.22	12.99	17.08	17.13	14.71	12.66	11.55	16.48	12.38	15.93	11.88	10.60	10.55
Na_2O	1.88	3.34	4.61	4.39	1.40	1.60	2.56	4.10	4.43	2.19	4.75	2.43	4.78	4.81	5.22
K_2O	<d.l.	0.18	0.32	0.30	0.20	0.10	0.18	0.20	0.22	0.16	0.22	0.13	0.23	0.27	0.27
Total	100.00	98.99	100.00	100.00	100.00	100.00	100.00	100.00	100.00	100.00	100.00	100.00	100.00	99.58	100.54
An%	82.38	68.75	58.32	61.03	86.05	85.04	75.18	62.29	58.25	79.86	58.31	77.78	57.10	54.01	51.93
Ab%	17.14	30.18	39.86	37.31	12.74	14.37	23.72	36.53	40.42	19.22	40.45	21.47	41.58	44.35	46.49
Or%	0.48	1.07	1.82	1.66	1.21	0.59	1.10	1.18	1.33	0.92	1.23	0.76	1.32	1.64	1.58
	Maca														
Method	EMP	EMP	EMP	SEM-EDS	SEM-EDS	EMP	EMP	SEM-EDS	SEM-EDS	SEM-EDS	SEM-EDS	SEM-EDS	SEM-EDS	SEM-EDS	SEM-EDS
Sample	PA-15 ph. core	PA-15 ph. rim	PA-15 ph. rim	PA-15 ph. core	PA-15 grm	PA-93 ph. core	PA-93 ph. rim	PA-93 grm	PA-85 ph. core	PA-85 ph. rim	PA-85 grm	PA-89 ph. core	PA-89 grm	PA-90 ph. core	PA-90 ph. rim
SiO_2	46.57	51.49	53.40	46.46	56.27	46.31	46.08	53.49	43.67	48.79	57.92	49.55	52.45	54.57	56.27
Al_2O_3	34.18	30.30	29.26	33.67	26.31	34.65	33.78	26.40	36.94	32.87	26.44	32.45	30.18	28.07	27.33
Fe_2O_3	0.62	0.79	0.86	0.79	1.63	0.46	0.73	2.96	0.85	0.62	0.88	0.52	0.69	0.72	0.48
CaO	17.17	13.10	12.29	17.16	9.37	17.47	17.07	12.21	16.95	15.66	8.25	14.87	12.62	10.76	9.65
Na_2O	1.50	3.81	4.37	1.92	5.84	1.32	1.55	4.54	1.39	1.81	6.05	2.61	3.94	5.58	6.05
K_2O	<d.l.	<d.l.	0.15	<d.l.	0.58	<d.l.	<d.l.	0.40	0.20	0.24	0.46	<d.l.	0.11	0.30	0.22
Total	100.04	99.49	100.33	100.00	100.00	100.21	99.21	100.00	100.00	100.00	100.00	100.00	100.00	100.00	100.00
An%	86.09	65.17	60.31	83.16	45.42	87.87	85.78	58.45	86.06	81.44	41.78	75.90	63.46	50.72	46.26
Ab%	13.61	34.30	38.81	16.84	51.24	12.01	14.10	39.28	12.72	17.07	55.44	24.10	35.88	47.60	52.48
Or%	0.30	0.53	0.88	0.00	3.34	0.12	0.12	2.27	1.21	1.49	2.79	0.00	0.66	1.69	1.26

Table 4
Selected analyses of Fe–Ti oxides

	Cay														
Method	SEM-EDS	SEM-EDS	SEM-EDS	SEM-EDS	SEM-EDS	SEM-EDS	SEM-EDS	SEM-EDS	SEM-EDS	SEM-EDS	SEM-EDS	SEM-EDS	SEM-EDS	SEM-EDS	SEM-EDS
Sample	PA-23 μph.	PA-23 grm	PA-23 grm	PA-23 μph.	PA-67 μph.	PA-67 μph.	PA-67 grm	PA-67 μph.	PA-67 μph.	PA-65 μph.	PA-65 μph.	PA-21 ph. core	PA-21 ph. rim	PA-21 μph.	PA-21 μph.
TiO_2	21.00	23.31	24.41	21.38	17.61	19.67	15.25	15.49	18.17	18.11	16.00	17.63	17.82	17.87	17.77
Al_2O_3	2.03	1.28	2.48	2.18	3.18	2.46	2.73	3.50	2.78	2.67	2.82	2.79	2.50	2.72	2.84
Cr_2O_3	0.13	0.13	<d.l.	<d.l.	0.31	0.41	<d.l.	0.24	0.27	0.11	<d.l.	<d.l.	<d.l.	0.19	<d.l.
FeO_{tot}	75.26	74.31	70.84	74.89	76.88	75.56	80.64	78.44	76.81	76.59	78.83	76.30	76.54	76.28	76.46
MnO	0.68	0.52	0.59	0.41	0.55	0.60	0.16	0.31	0.58	0.81	0.80	0.80	0.70	0.85	0.68
MgO	0.90	0.45	1.68	1.14	1.47	1.30	1.22	2.02	1.39	1.71	1.55	2.48	2.44	2.09	2.25
Total	100.00	100.00	100.00	100.00	100.00	100.00	100.00	100.00	100.00	100.00	100.00	100.00	100.00	100.00	100.00
Usp%	57.0	63.8	65.9	57.8	47.2	53.0	40.9	41.2	48.8	48.6	42.8	46.8	47.5	47.8	47.4
Mt%	43.0	36.2	34.1	42.2	52.8	47.0	59.1	58.8	51.2	51.4	57.2	53.2	52.5	52.2	52.6
	Maca											Bahia Pérez			
Method	SEM-EDS	SEM-EDS	SEM-EDS	SEM-EDS	SEM-EDS	SEM-EDS	SEM-EDS	SEM-EDS	SEM-EDS	SEM-EDS	SEM-EDS	EMP	EMP	SEM-EDS	SEM-EDS
Sample	PA-15 μph.	PA-15 μph.	PA-15 grm	PA-93 grm	PA-93 μph.	PA-93 grm	PA-85 μph.	PA-85 μph.	PA-90 μph.	PA-90 grm	PA-90 μph.	PA-71 grm	PA-71 grm	PA-71 #	PA-71 #
TiO_2	14.28	20.16	22.47	16.42	19.96	22.32	13.97	14.38	16.63	21.10	16.27	17.42	16.52	0.73	0.78
Al_2O_3	2.77	2.67	0.97	3.27	3.94	2.04	3.92	3.01	2.81	1.71	2.91	3.07	3.07	30.70	30.92
Cr_2O_3	9.84	0.12	0.12	0.19	0.31	0.35	0.12	0.18	<d.l.	<d.l.	0.15	<d.l.	<d.l.	28.11	28.55
FeO_{tot}	70.67	74.43	74.37	76.61	70.91	71.92	79.06	79.27	77.51	74.31	77.91	74.74	73.76	24.97	24.04
MnO	0.48	0.40	0.61	0.76	0.60	0.57	0.67	0.87	0.82	1.09	0.94	<d.l.	<d.l.	<d.l.	<d.l.
MgO	1.96	2.22	1.46	2.75	4.28	2.80	2.26	2.29	2.23	1.79	1.82	1.18	1.79	15.49	15.71
Total	100.00	100.00	100.00	100.00	100.00	100.00	100.00	100.00	100.00	100.00	100.00	96.41	95.14	100.00	100.00
Usp%	38.3	54.0	61.1	43.5	52.3	59.8	37.0	38.2	44.3	56.8	43.5	59.2	60.8		
Mt%	61.7	46.0	38.9	56.5	47.7	40.2	63.0	61.8	55.7	43.2	56.5	40.8	39.2		

#: Cr-spinel included in olivine phenocrysts.

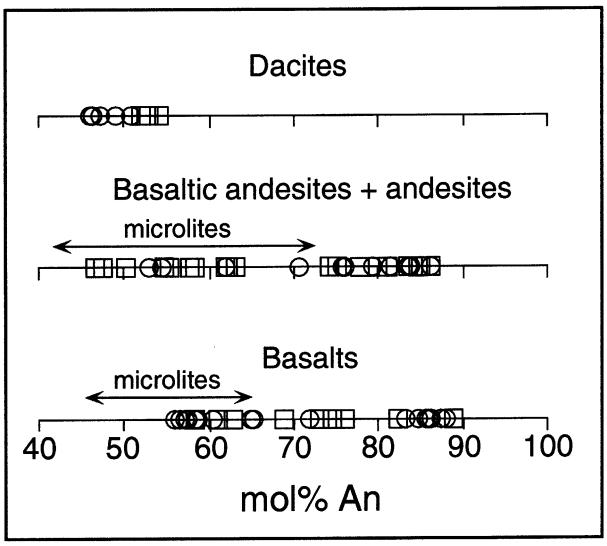

Fig. 5. Plagioclase phencrysts composition (An mol%) in the Cay (squares) and Maca (circles) basalts, basaltic andesites + andesites, and dacites. Arrows indicate the compositional range for the groundmass microlites.

plagioclase + olivine ± Ti-magnetite ± pyroxene, joined by apatite for magmas with $SiO_2 > 60$ wt%. This interpretation is supported by the ubiquitous occurrence of olivine + plagioclase ± pyroxene ± Ti-magnetite glomerophyric aggregates in the more primitive rocks and of plagioclase + pyroxene ± Ti-magnetite ± apatite aggregates in dacite rocks.

5.2. Trace elements and Sr–Nd isotopes

The volcanic rocks of this study share a marked arc-type, incompatible element distribution. In the primordial mantle-normalized plot (Fig. 8), basalt to dacite rocks from Maca, Cay, and Bahia Pérez are characterized by variable enrichments of large ion lithophile elements (LILE; e.g. Cs, Rb, Ba, K), as well as Pb, Th, and U over high field strength elements (HFSE; e.g. Nb, Ta, Zr, Hf, Ti), as is commonly observed for subduction-related magmas. The contents of the most incompatible elements exhibit a strong positive correlation with the SiO_2 concentration, whereas the 3rd transition elements (Sc, V, Cr, Co, Ni) and Sr decrease as the silica content increases (Table 5, Fig. 9).

Chondrite-normalized rare earth element (REE) patterns are slightly LREE enriched ($[La/Yb]_N = 2.6–5.7$) and do not differ significantly in their shape (Fig. 10). Dacites from Maca and Cay (plus the Maca andesite PA-89) are characterized by detectable negative Eu anomalies ($[Eu/Eu^*] = 0.75–0.85$). In addition, the dacites from Cay exhibit a slightly higher LREE/HREE fractionation (Fig. 10).

In Harker's diagrams (Fig. 9), samples from the Hudson volcano are characterized by remarkably higher Nb and Zr and, to a lesser extent, Rb and Y contents in comparison with samples from the Cay and Maca volcanoes.

The isotopic compositions of Sr and Nd were determined for 12 whole-rock samples (Table 6). The whole range of $^{87}Sr/^{86}Sr$ and $^{143}Nd/^{144}Nd$ values is remarkably narrow (0.70389–0.70431 and 0.51277–0.51284, respectively). In the Sr–Nd isotope space (Fig. 11), the volcanics fall in the central portion of the field that encloses the volcanic rocks from the SSVZ. In Fig. 12, in which the $^{87}Sr/^{86}Sr$ ratios of the Cay, Maca, Bahia Pérez, and Hudson volcanics are plotted against their SiO_2 content, we can observe the following: (1) basaltic rocks show Sr-isotope compositions that encompass the observed range of $^{87}Sr/^{86}Sr$ values (0.7039–0.7045); (2) except for sample PA-71 from Bahia Pérez, basaltic andesites, andesites, and dacites show $^{87}Sr/^{86}Sr$ values greater than 0.7041; and (3) within the evolutionary series of each volcano, no clear correlation between $^{87}Sr/^{86}Sr$ and SiO_2 is observed.

The crustal contamination of the basalt with the lowest $^{87}Sr/^{86}Sr$ ratio (PA-22 from Cay) has been modeled in terms of simple binary mixing with a hypothetical Andean

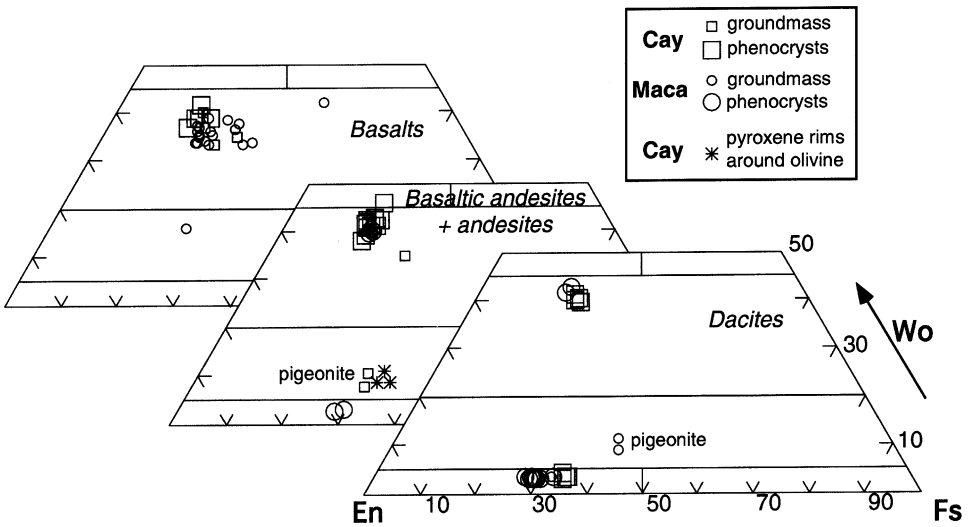

Fig. 6. Pyroxene compositional data for the Cay and Maca volcanics plotted in the Di–Hd–En–Fs quadrilateral.

Table 5
Major- and trace-element data for selected volcanic rocks from the Cay and Maca volcanoes and Bahia Pérez parasitic cones

Locality	Cay										Maca										Bahia Pérez		
Sample	PA-22	PA-23	PA-67	PA-70	PA-20C	PA-69	PA-65	PA-66	PA-21	PA-24	PA-93	PA-15	PA-14	PA-19M	PA-92	PA-62	PA-85	PA-89	PA-90	PA-88	PA-71	PA-74	PA-77
Rock	B	B	BA	BA	A	A	A	A	D	D	B	B	B	B	BA	BA	BA	A	D	D	B	BA	A
SiO_2 (wt%)	50.63	50.65	53.85	54.07	55.58	57.50	58.20	58.78	65.48	65.65	49.86	50.11	50.79	50.79	51.97	52.93	55.02	56.53	62.81	63.55	50.90	52.47	56.37
TiO_2	1.07	1.01	1.08	1.08	1.47	1.11	1.22	1.24	0.86	0.65	1.01	1.08	1.05	1.14	1.06	1.00	1.26	0.89	1.08	1.00	1.04	1.10	1.20
Al_2O_3	18.37	18.24	19.61	17.59	15.65	17.94	17.16	17.22	15.48	16.47	19.25	20.27	18.69	17.51	18.01	18.09	17.34	17.51	15.59	15.92	16.87	18.70	16.88
Fe_2O_3	3.46	2.17	3.15	7.93	2.96	2.02	2.72	3.33	1.57	1.85	6.93	3.49	2.78	2.70	3.56	4.15	3.93	3.69	1.63	1.48	1.94	3.74	2.73
FeO	5.32	6.64	5.12	1.18	6.80	5.14	4.71	4.09	3.40	2.50	2.65	5.40	6.20	6.86	5.76	4.25	5.26	4.14	3.98	3.89	6.74	5.19	5.40
MnO	0.14	0.14	0.14	0.14	0.18	0.16	0.17	0.17	0.12	0.14	0.15	0.14	0.15	0.16	0.15	0.13	0.17	0.14	0.16	0.16	0.15	0.15	0.16
MgO	5.79	6.28	3.88	4.62	3.18	2.57	2.66	2.67	1.37	1.12	5.33	4.19	5.35	6.36	5.12	5.17	3.22	4.12	1.69	1.68	8.17	4.11	3.41
CaO	9.82	10.04	9.31	8.39	6.46	6.54	5.89	5.80	3.62	3.12	10.05	9.95	9.97	9.67	9.72	8.90	7.21	7.58	3.95	3.99	9.16	9.39	7.16
Na_2O	3.16	3.09	3.63	3.67	4.38	4.63	5.07	4.93	4.82	5.45	2.99	3.31	3.19	3.14	3.36	3.32	4.39	3.60	5.31	5.50	3.10	3.46	4.32
K_2O	0.78	0.74	0.72	0.97	1.08	1.15	1.24	1.25	2.48	2.32	0.48	0.48	0.57	0.58	0.59	0.93	0.77	0.92	1.90	1.73	0.66	0.61	1.07
P_2O_5	0.19	0.19	0.23	0.22	0.29	0.26	0.34	0.31	0.25	0.20	0.19	0.16	0.19	0.21	0.17	0.19	0.23	0.16	0.35	0.29	0.24	0.18	0.27
LOI	0.69	0.88	0.32	0.31	0.93	0.54	0.29	0.50	0.54	0.44	0.61	1.12	0.93	0.77	0.56	1.05	0.44	1.53	1.91	0.64	0.71	0.54	0.95
Total	99.42	100.07	101.04	100.17	98.96	99.56	99.67	100.29	99.99	99.91	99.50	99.70	99.86	99.89	100.03	100.11	99.24	100.81	100.36	99.83	99.68	99.64	99.92
Sc (ppm)	31	32	28	29	26	23	24		14	10	31		26		34	26	30	24	19	17	28	30	26
V	261	271	253	242		133	142		69	18	259				295	227	236	233	68	57	232	262	218
Cr	85	101	38	55	2	5	2		3	1	53		42		54	63	6	28	2	2	285	29	14
Co	41	37	26	29		14	15		9	5	39				38	35	22	25	8	8	38	27	21
Ni	39	44	16	24	9	4	3		2	1	25		26		19	29	6	16	5	2	140	15	8
Rb	11.6	10.1	13.7	20.5	27.2	25.2	23.1		68	55	11.4		15.4		11.8	23.4	15.2	23.6	46	39	11.0	12.7	23.2
Sr	662	663	565	467	459	498	501		325	372	512		570		531	483	498	456	367	397	534	490	565
Y	19.4	18.0	22.5	24.8	29.0	32	33		36	32	19.7		17.7		20.0	23.0	26.7	24.6	43	37	20.7	20.9	27.0
Zr	81	75	97	121	123	141	156		221	230	69		69		66	99	88	107	213	176	91	71	113
Nb	2.40	2.17	3.0	3.6	4.3	4.0	5.2		6.2	6.5	2.28		2.47		1.84	3.4	2.75	3.0	6.7	6.4	3.1	2.16	3.2
Cs	0.43	0.37	0.55	0.47	1.76	1.25	0.49		2.74	2.00	0.84		0.94		1.00	1.04	0.47	1.77	3.5	2.96	0.60	1.02	1.39
Ba	228	213	237	286	327	336	369		555	642	157		173		173	248	249	314	495	451	203	175	290
La	9.7	8.8	11.1	13.4	14.0	15.1	17.3		23.5	26.9	7.9		7.8		7.0	11.1	9.7	16.2	23.0	18.5	11.1	7.2	12.5
Ce	24.2	20.8	26.5	30	34	36	41		52	61	19.5		19.6		17.2	27.2	23.6	32	53	45	26.7	17.9	29.9
Pr	3.5	3.0	3.7	4.2	4.8	5.0	5.7		7.0	7.8	2.87		2.82		2.58	3.7	3.5	4.4	7.3	6.2	3.8	2.59	4.2
Nd	15.1	13.7	15.7	17.9	21.2	21.3	23.9		28.2	29.5	12.7		12.7		11.6	16.1	15.8	19.2	30	26.3	15.9	12.5	18.6
Sm	3.6	3.4	3.7	4.2	5.2	5.0	5.6		6.1	6.0	3.4		3.1		3.2	3.9	4.1	3.9	7.0	6.3	3.7	3.2	4.5
Eu	1.17	1.14	1.25	1.25	1.68	1.57	1.68		1.50	1.51	1.06		1.13		1.08	1.13	1.38	1.13	1.93	1.70	1.19	1.13	1.46
Gd	3.8	3.6	3.7	4.4	5.6	5.1	5.5		6.1	5.3	3.5		3.6		3.6	3.9	4.2	4.4	6.9	6.5	3.4	4.0	4.5
Tb	0.57	0.53	0.65	0.71	0.86	0.92	0.94		0.98	0.87	0.57		0.53		0.58	0.66	0.73	0.66	1.19	1.04	0.59	0.63	0.77
Dy	3.4	3.2	3.7	4.2	5.3	5.3	5.5		5.9	5.1	3.5		3.4		3.5	3.9	4.5	4.1	7.2	6.3	3.4	3.7	4.5
Ho	0.67	0.62	0.77	0.83	1.06	1.12	1.16		1.18	1.09	0.70		0.64		0.72	0.83	0.94	0.83	1.47	1.32	0.73	0.76	0.92
Er	1.89	1.72	2.13	2.34	2.97	3.1	3.2		3.4	3.3	2.03		1.79		2.05	2.35	2.52	2.20	4.1	3.9	1.94	2.15	2.53
Tm	0.28	0.25	0.32	0.34	0.43	0.44	0.47		0.52	0.50	0.28		0.26		0.30	0.34	0.37	0.35	0.63	0.55	0.27	0.31	0.36
Yb	1.70	1.53	1.94	2.16	2.83	2.85	2.92		3.3	3.2	1.76		1.69		1.78	2.09	2.34	2.20	3.8	3.3	1.75	1.93	2.35
Lu	0.23	0.21	0.30	0.31	0.43	0.45	0.47		0.48	0.47	0.25		0.26		0.26	0.30	0.37	0.32	0.59	0.51	0.27	0.29	0.35
Hf	2.14	1.94	2.36	2.99	3.4	3.6	3.8		5.6	5.8	1.93		1.89		1.93	2.77	2.40	2.80	5.2	4.9	2.18	2.01	2.94
Ta	0.15	0.14	0.19	0.24	0.26	0.29	0.32		0.46	0.45	0.13		0.15		0.12	0.23	0.18	0.22	0.44	0.42	0.18	0.14	0.22
Pb	4.8	3.7	4.5	6.4	10.5	7.7	17.9		15.2	15.2	5.2		5.3		6.2	7.7	5.6	7.6	16.0	14.8	4.8	4.4	7.0
Th	2.05	1.51	1.28	2.06	2.08	2.48	2.09		6.1	5.5	0.93		1.08		1.00	3.2	1.12	4.6	5.0	4.9	1.38	0.86	2.22
U	0.53	0.44	0.39	0.58	0.84	0.66	0.62		1.64	1.52	0.34		0.43		0.48	0.99	0.45	1.14	1.49	1.67	0.37	0.40	0.62

B: calc-alkaline basalt; BA: basaltic andesite; A: andesite; D: dacite. Blank: not determined, LOI: loss on ignition.

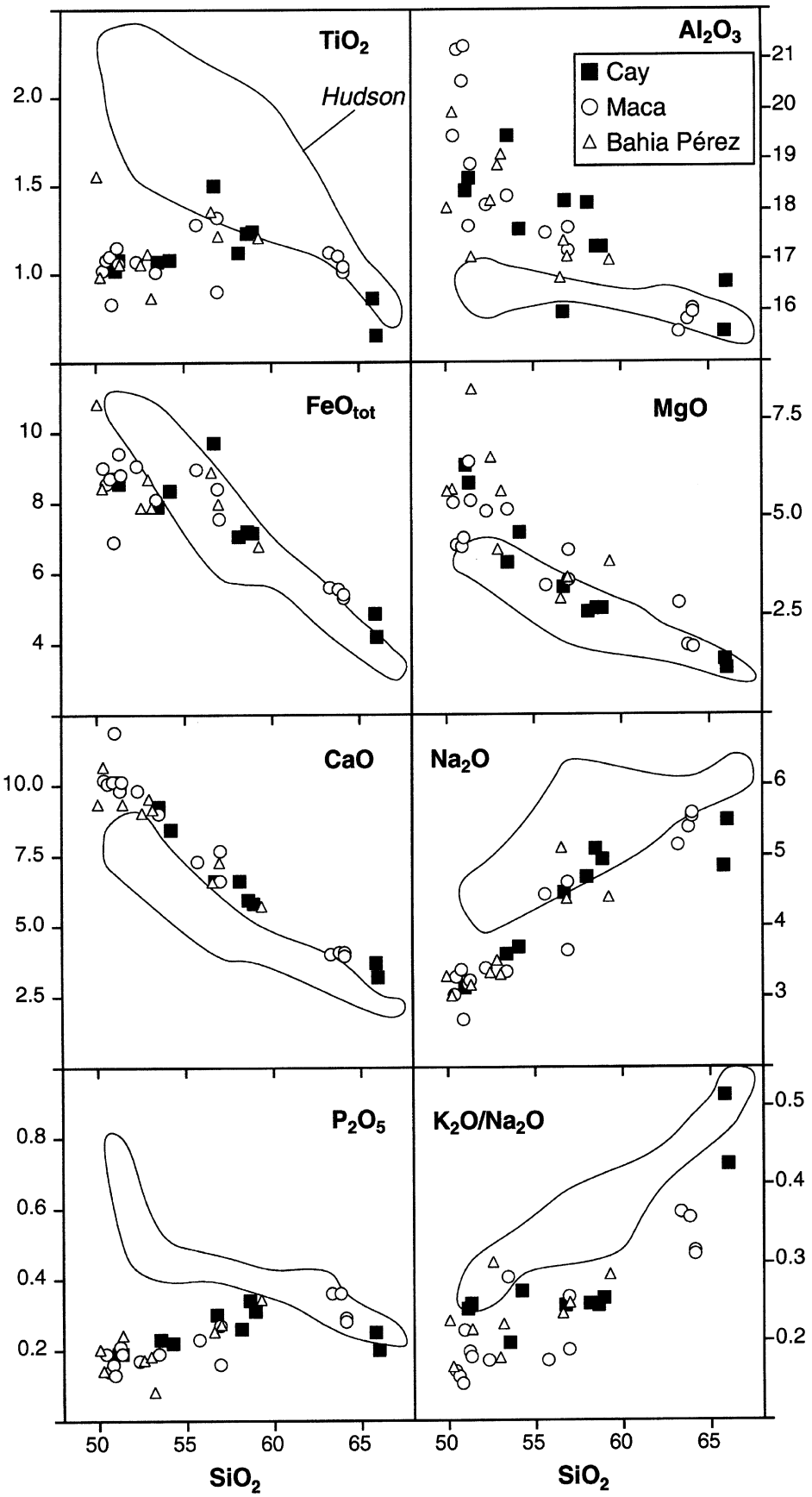

Fig. 7. Major-element (wt%) Harker's diagrams for the Cay, Maca, and Bahia Pérez volcanics.

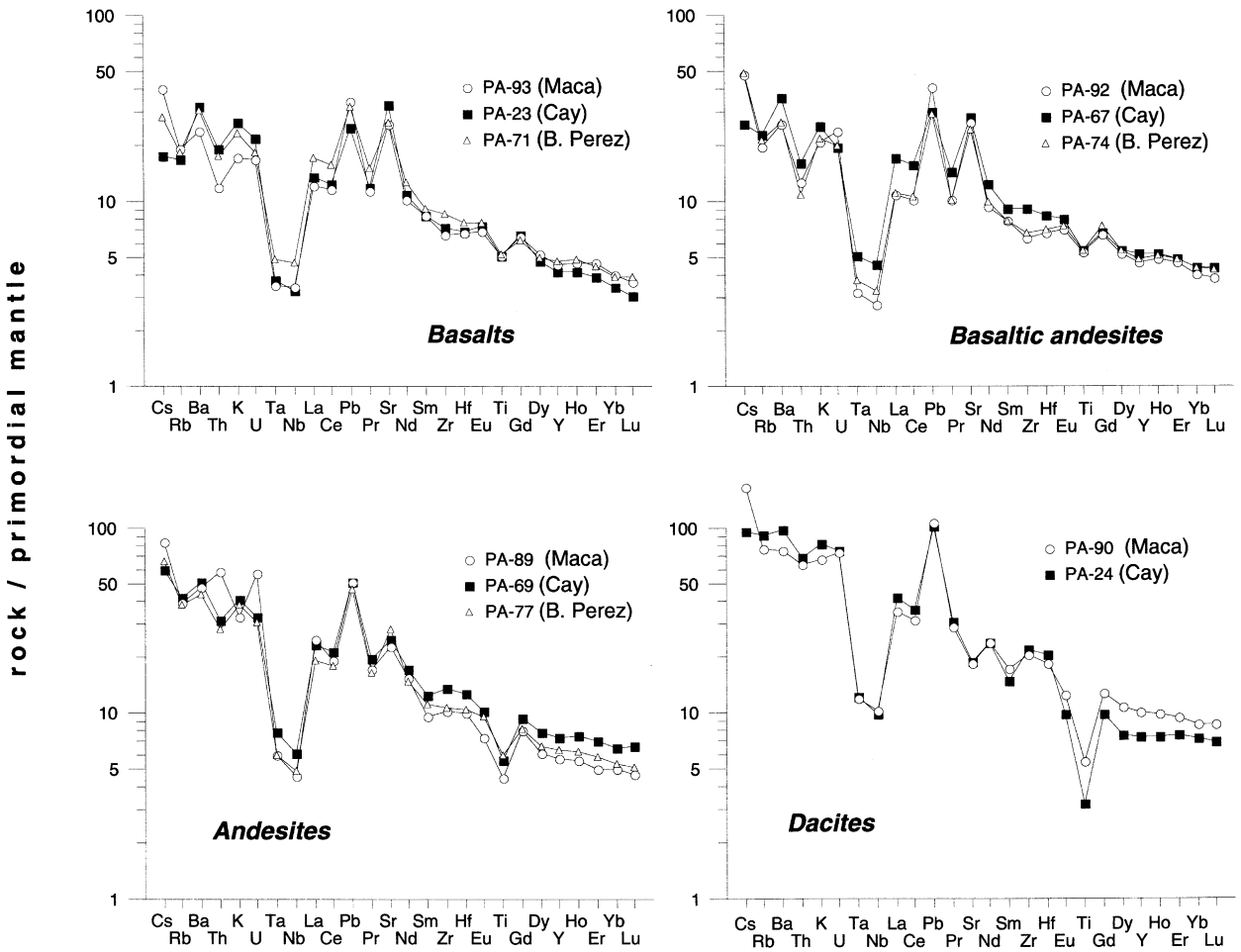

Fig. 8. Primordial, mantle-normalized, incompatible element diagrams for selected basalt, basaltic andesite, andesite, and dacite rocks from Cay, Maca, and Bahia Pérez. Normalizing values are after McDonough and Sun (1995).

basement (Stern and Kilian, 1996) or the average lower continental crust (Taylor and McLennan, 1985) and in terms of assimilation plus fractional crystallization processes. The results of the modeling, plotted in a $^{87}Sr/^{86}Sr$ versus Ba/Zr diagram (Fig. 13), indicate that crustal contamination was only a minor cause of the isotopic variability of the volcanics from the Maca/Cay/Hudson region. In particular, basalts that show small differences in their Sr–Nd isotope compositions probably originated in a slightly geochemically heterogeneous mantle.

6. Estimates of T, fO_2 and H_2O content

Temperatures of phenocryst equilibration were estimated using the QUILF program (Andersen et al., 1993) and pyroxene (augite, orthopyroxene, or augite + orthopyroxene) compositions. The olivine-basalt PA-71 from Bahia Pérez contains equilibrium olivine phenocrysts with homogeneous cores and Cr-spinel inclusions. The crystallization temperature of this sample was calculated from olivine–liquid (Leeman and Scheidegger, 1977) and olivine-spinel (Sack and Ghiorso, 1991) equilibria. The results (Table 7) indicate phenocryst equilibration temperature ranges of 1210–1125 °C for basalts, 1170–1100 °C for basaltic andesites and andesites, and 1070–1010 °C for dacites.

Oxygen fugacities were also estimated using the QUILF program. Only the composition of the Ti-magnetite microphenocrysts is needed for the calculation, because the temperature is constrained by the pyroxene composition (Table 7). The results indicate reasonably high values of the relative oxygen fugacities 1.2–2.2 log units above the QFM (quartz–fayalite–magnetite) buffer and no systematic relationship between fugacity and whole-rock composition or temperature.

An estimate of the preeruptive magmatic water content of the low porphyricity (< 10 vol% phenocrysts) lavas from Cay and Maca was attempted using the plagioclase-hydrous melt equilibrium relationships developed by Housh and Luhr (1991), with the compositions of whole-rocks and plagioclase phenocryst cores as input data. We assumed

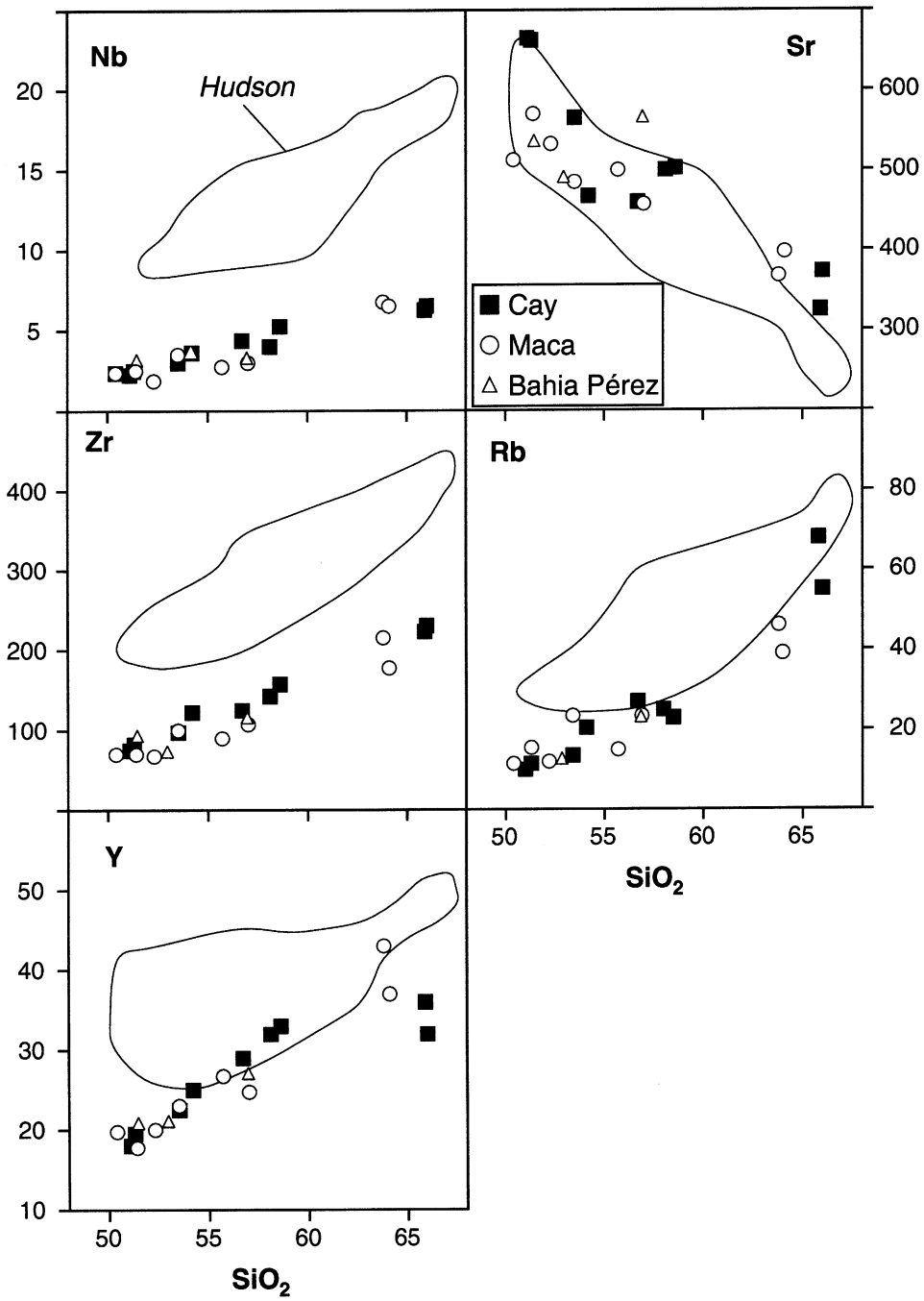

Fig. 9. Trace-element (ppm) Harker's diagrams for the Cay, Maca, and Bahia Pérez volcanics.

that, for low porphyricity lavas, the cores of plagioclase phenocrysts grew in equilibrium at the temperature constrained by pyroxene thermometry, with a melt whose composition is the same as that of the whole rock. The results indicate H_2O contents vary between 1.8 and 5.3 wt%. The highest value was calculated for the andesite lava PA-65, which contains plagioclase phenocrysts with high An content (up to An_{85}), and the lowest values were estimated for the dacite samples.

7. Discussion

7.1. Fractional crystallization in the Cay and Maca lavas

The new data reported in this study indicate that volcanic rocks occurring in the Cay and Maca volcanic regions share similar petrographical and geochemical features and define typical calc-alkaline trends from subalkaline basalts to dacites.

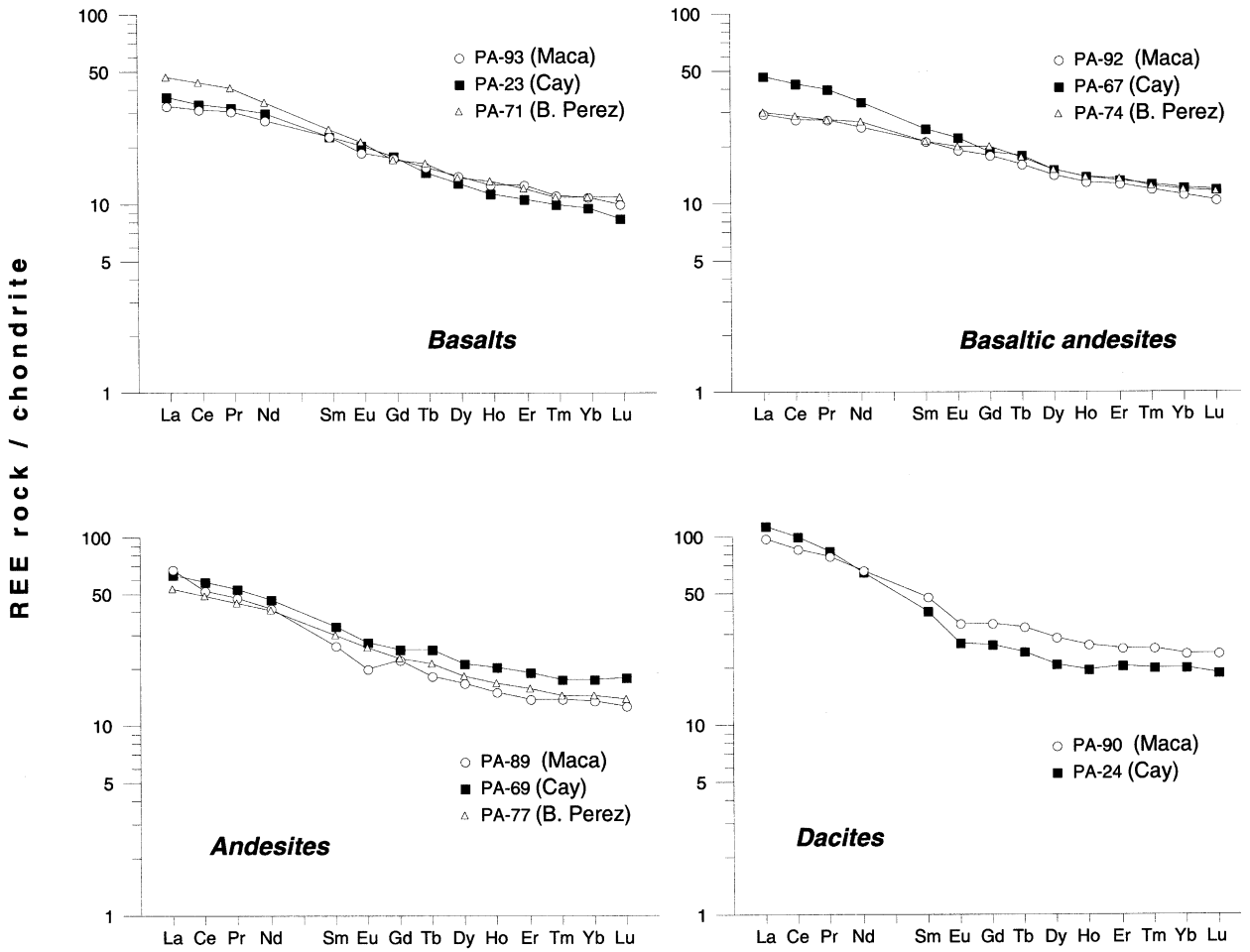

Fig. 10. Chrondrite-normalized REE patterns for selected basalt, basaltic andesite, andesite, and dacite rocks from Cay, Maca, and Bahia Pérez. Normalizing values are after McDonough and Sun (1995).

The reduced Sr–Nd isotope variability and continuity of chemical variation trends suggest a prevailing closed system evolution of magmas by fractional crystallization without significant interaction with the crust beneath the volcanoes. Simple mass-balance calculations, using the compositions of whole rocks and their phenocryst phases as input data, indicate that dacites can be obtained from basalt parent magmas by fractionating a total of ~70 wt% of a solid assemblage dominated by plagioclase plus pyroxene, olivine, Ti-magnetite, and apatite. For example, Table 8

Table 6
Sr–Nd isotope data

Locality	Sample	Rock type	$^{87}Sr/^{86}Sr$	$\pm 2\sigma_{mean}$	$^{143}Nd/^{144}Nd$	$\pm 2\sigma_{mean}$
Maca	PA-93	B	0.704232	12	0.512817	10
Maca	PA-15	B	0.704250	15	0.512808	14
Maca	PA-85	BA	0.704288	12	0.512808	12
Maca	PA-89	A	0.704306	12	0.512768	10
Maca	PA-86	D	0.704099	11	0.512838	10
Maca	PA-88	D	0.704092	10	0.512820	11
Cay	PA-22	B	0.703888	10	0.512813	10
Cay	PA-67	BA	0.704170	10	0.512797	13
Cay	PA-65	A	0.704111	15	0.512812	10
Cay	PA-24	D	0.704208	13	0.512777	10
Bahia Pérez	PA-71	B	0.704167	13	0.512794	10
Bahia Pérez	PA-77	A	0.703918	10	0.512813	15

B: calc-alkaline basalt; BA: basaltic andesite; A: andesite; D: dacite.

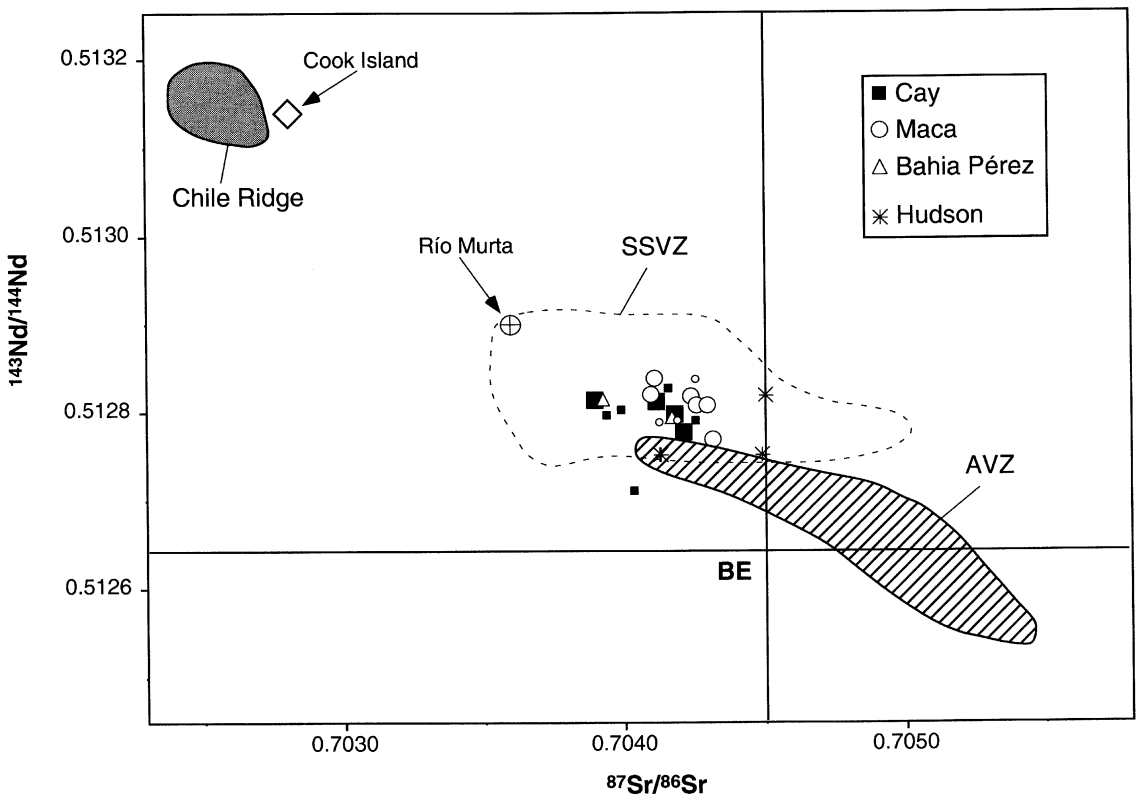

Fig. 11. $^{143}Nd/^{144}Nd$ versus $^{87}Sr/^{86}Sr$ diagram for the Cay, Maca, and Bahia Pérez volcanics (smaller symbols indicate values for Cay and Maca from the literature). Also shown are the fields for the Chile ridge (Klein and Karsten, 1995; Bach et al., 1996), the AVZ (excluding Cook Island), and the other volcanoes of the SSVZ (excluding the Husdon) (Hickey-Vargas et al., 1986, 1989; Gerlach et al., 1988; Futa and Stern, 1988; Lopez-Escobar et al., 1993, 1995a,b; Stern and Kilian, 1996; Naranjo and Stern, 1998). Legend: asterisk, Husdon volcano; crossed circle, Río Marta basalt (Demant et al., 1998); diamond, Cook Island; BE, bulk Earth.

shows the results of the major-element least squares mass-balance calculations for the crystal fractionation of the Cay magmas for the transitions from basalt PA-23 to andesite PA-69 and from the latter to dacite PA-21.

The fraction of remaining magma (F) and the predicted fractionating solid assemblages obtained from the major-element mass-balance were used as input data in trace-element Rayleigh fractionation modeling. Elemental partition coefficients for 31 trace elements used in the calculations were obtained from the Geochemical Earth Reference Model database (http://www.earthref.org/database/KDD). Table 8 reports the observed and calculated trace-element compositions of the daughter magmas for the two fractionating steps. The trace-element concentrations of andesite PA-69 are well reproduced by the model with the notable exceptions of Cs, Rb, and Pb, whose observed concentrations are significantly higher than calculated. The results for dacite PA-21 are slightly worse. In particular, the observed HREE concentrations are lower than the calculated concentrations. The relatively low HREE concentrations of dacite PA-21 compared with those predicted by the model could be due to higher amounts of fractionated apatite or a stronger partitioning of HREE in apatite and clinopyroxene.

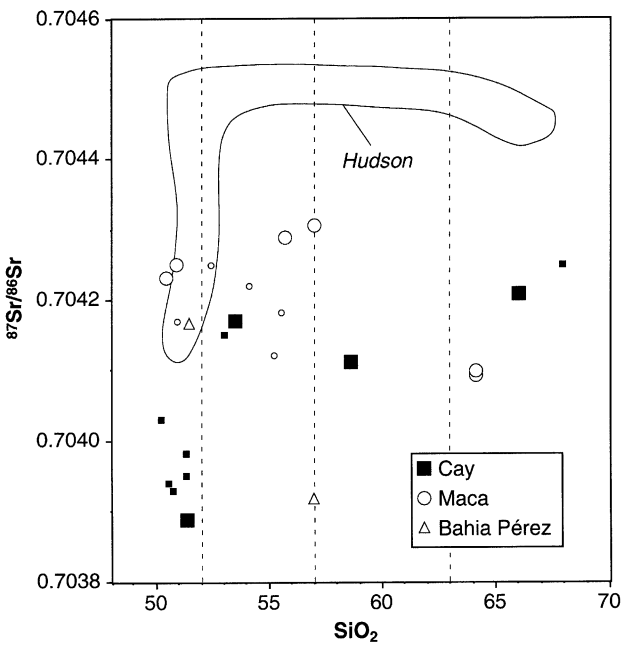

Fig. 12. $^{87}Sr/^{86}Sr$ versus SiO_2 (wt%) diagram for the Cay, Maca, Bahia Pérez, and Hudson volcanics. The vertical dashed lines are from the SiO_2 contents delimiting basalt, basaltic andesite, andesite, and dacite fields in the K_2O versus SiO_2 classification program (Peccerillo and Taylor, 1976). Symbols are as in Fig. 11.

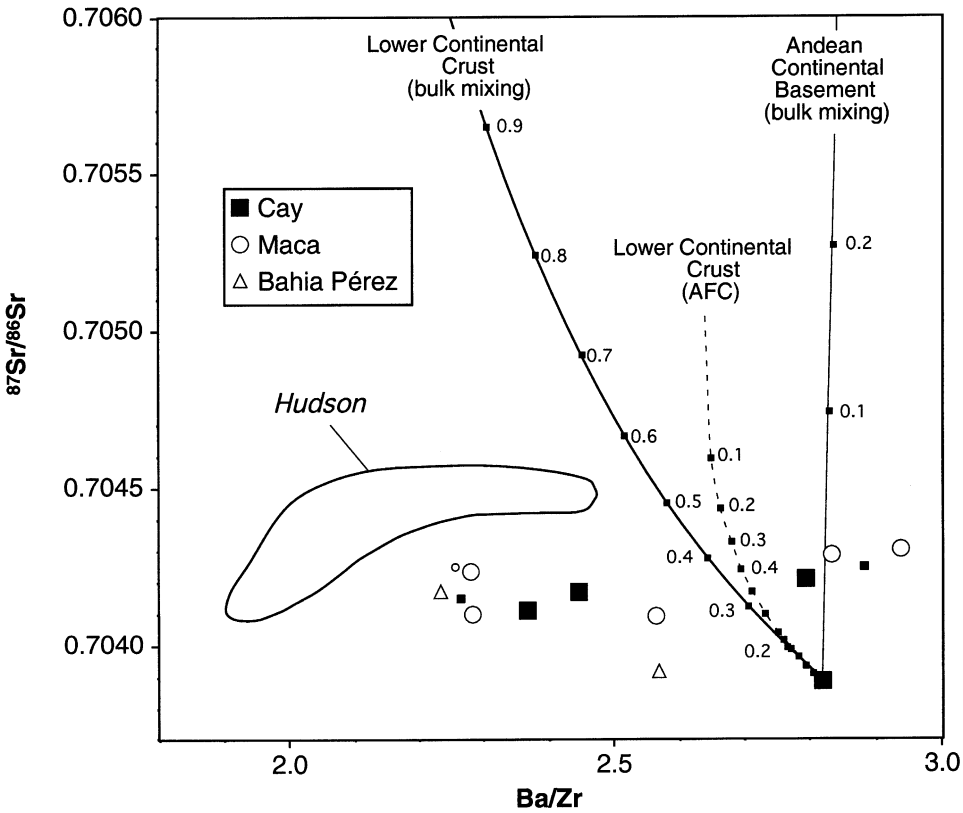

Fig. 13. $^{87}Sr/^{86}Sr$ versus Ba/Zr diagram for the Cay, Maca, Bahia Pérez, and Hudson volcanics. Also plotted are the binary mixing lines (numbers refer to the weight fraction of assimilated materials) between Cay basalt PA-22 ($^{87}Sr/^{86}Sr = 0.70389$, Sr = 662 ppm, Ba = 228 ppm, Zr = 81 ppm) and the lower continental crust composition (Taylor and McLennan, 1985) (Sr = 230 ppm, Ba = 150 ppm, Zr = 70 ppm; assumed $^{87}Sr/^{86}Sr = 0.707$) and the Andean continental basement (Stern and Kilian, 1996) ($^{87}Sr/^{86}Sr = 0.715$, Sr = 220 ppm, Ba = 485 ppm, Zr = 170 ppm), which is a 1:1 mixture of South American metamorphic basement (S-type) and Patagonian batholith (I-type). In addition, there is a plot for the curve (dashed line; numbers refer to the fraction of remaining magma) obtained for the assimilation plus fractionalized crystallization (AFC) from Cay basalt PA-22 assuming the lower continental crust as a contaminant, an r value (ratio between assimilation and fractional crystallization rates) of 0.3, and bulk partition coefficients for Sr, Ba, and Zr of 0.6, 0.0, and 0.0, respectively. Symbols are as in Fig. 11.

As already observed for the fractionation from basalt to andesite, the observed contents of Cs, Rb, and Pb are higher than calculated. It is thus likely that the concentration of these highly mobile elements was modified by processes (e.g. weathering) other than crystal fractionation.

7.2. Evaluation of subduction-derived components

The compositions of magmas erupted at convergent plate margins indicate that their mantle sources were modified by the addition of materials derived from the subducting slab. These materials can be hydrous fluids released from the subducted oceanic crust, subducted sediments, or silicate liquids derived from slab melting.

The Cay and Maca volcanic region is located between the on-land projections of the Darwin and Guamblin oceanic fracture zones (Fig. 1). Between these fracture zones, the oceanic crust entering the Chile trench has an age of ~3 Ma (anomaly 2A). With a slab dip of ≈25° (Cahill and Isacks, 1992), the subducting lithosphere beneath the Cay and Maca volcanoes should be <10 Ma, and its top should be ~110 km deep. Such a young (and hot) subducting lithosphere can yield slab melts (Peacock et al., 1994). The Sr/Y versus Y diagram (Fig. 14) has been used to discriminate magmas that bear a slab melt or adakitic signature from normal arc magmas. Melts from

Table 7
Estimates of pre-eruptive temperature and fO_2

	Rock type	T (°C)	Geothermometer	fO_2 (log units above QFM)
PA-71	B	1210–1215	Ol-Liq[a]	
PA-71	B	1153	Ol-Sp[b]	
PA-23	B	1125–1165	QUILF-cpx[c]	
PA-67	BA	1115–1150	QUILF-cpx	1.4–1.9
PA-85	BA	1100–1120	QUILF-opx	2.1–2.2
PA-65	A	1105–1170	QUILF-cpx	1.5–1.8
PA-90	D	1020–1065	QUILF-cpx/opx	1.7
PA-21	D	1010–1070	QUILF-cpx/opx	1.3–1.5

[a] Olivine–liquid geothermometer of Leeman and Scheidegger (1977).
[b] Olivine–spinel geothermometer of Sack and Ghiorso (1991).
[c] One- or two-pyroxenes geothermometer of Andersen et al. (1993).

Table 8
Major-element least squares mass-balance calculations and trace-element Rayleigh fractionation modelling

Parent	PA-23	Basalt	PA-69	Andesite
Daughter	PA-69	andesite	PA-21	Dacite
SiO_2 range	51.2–58.2		58.2–66.0	
Ol (wt%)	6.8 (Fo_{81})		–	
Cpx	12.7 ($Wo_{39}En_{46}$)		9.0 ($Wo_{42}En_{41}$)	
Plag	26.7 (An_{82})		27.2 (An_{55})	
Ti-Mag	3.2 (Usp_{38})		4.0 (Usp_{47})	
Ap	-		0.3	
F	0.505		0.594	
$\sum r^2$	0.10		0.77	
	PA-69 obs.	PA-69 calc.	PA-21 obs.	PA-21 calc.
Sc (ppm)	23	25	14	13
V	133	133	69	56
Cr	5	5	3	1
Co	14	14	9	6
Ni	4	4	2	2
Rb	25	19	68	41
Sr	498	505	325	343
Zr	141	136	221	219
Nb	4.0	4.1	6.2	6.4
Cs	1.3	0.7	2.7	2.1
Ba	336	340	555	508
Hf	3.6	3.6	5.6	5.7
Ta	0.29	0.26	0.46	0.46
Pb	7.7	6.8	15.2	12.2
Th	2.5	2.8	6.1	4.1
U	0.66	0.76	1.64	1.10
La	15.1	14.9	23.5	21.0
Ce	36	35	52	49
Pr	5.0	5.0	7.0	6.6
Nd	21.3	22.5	28.2	27.4
Sm	5.0	5.5	6.1	6.1
Eu	1.57	1.52	1.50	1.70
Gd	5.1	6.1	6.1	6.4
Tb	0.92	0.89	0.98	1.18
Dy	5.3	5.3	5.9	6.9
Ho	1.12	1.06	1.18	1.52
Y	32	31	36	44
Er	3.1	3.0	3.4	4.3
Tm	0.44	0.45	0.52	0.64
Yb	2.9	2.6	3.3	4.0
Lu	0.45	0.37	0.48	0.66

Ol: olivine; Cpx: clinopyroxene; Plag: plagioclase; Ti-Mag: Ti-magnetite; p: apatite. F : weight fraction of remaining magma; $\sum r^2$: sum of squares of residuals. Sample and mineral analyses were recalculated to 100% before modelling.

the subducting oceanic crust are thought to be in equilibrium with garnet- or amphibole-bearing residues and therefore should be depleted in HREE. Volcanic rocks from Cay, Maca, and Bahia Pérez, as well as from the other volcanoes of the SSVZ, fall in a portion of the diagram (Fig. 14) distinct from that occupied by the adakitic rocks of the AVZ, for which a slab-melting origin has been proposed (Futa and Stern, 1988; Stern and Kilian, 1996; Sigmarsson et al., 1998). Moreover, magmas erupted in the studied region are characterized by only slightly fractionated REE patterns (Fig. 10) and MgO/FeO* ratios distinctly lower than those of typical adakitic rocks with a similar degree of evolution (Fig. 3). In conclusion, there is no geochemical evidence for the role of slab melt-type materials in the source of the volcanic rocks studied. Two types of subduction-derived materials therefore should be taken into account in the metasomatism of the Cay/Maca/Bahia Pérez mantle magma source: fluids and subducted sediments.

Decoupling incompatible trace elements with differential mobility in fluids and melts can enable us to understand specific subduction processes. Elements such as Cs, Rb, Sr, Ba, Pb, and B (fluid mobile elements [FME]) are preferentially partitioned in the fluid phase with respect to elements such as Zr, Ti, Nb, Ta, and REE. Thus, fluids released during the dehydration reactions in the subducted sediments and/or altered oceanic crust are characterized by high ratios between FME and other incompatible elements. In Fig. 15, the Ba/La ratios of our samples are plotted against their $^{87}Sr/^{86}Sr$ ratios. The model calculations, showing the bulk mixing between a preenrichment mantle source (depleted mantle; Hofmann, 1988) and the global subducted sediment (GLOSS; Plank and Langmuir, 1998), as well as a fluid phase proposed by Leeman et al. (1994), are also plotted in the diagram. The compositions of the volcanics studied can be reproduced by adding less than 1 wt% of a combination of fluids and sediments (in approximately equal proportions) to a depleted mantle source. The results of these calculations are simply qualitative because of the large uncertainty in the actual end-member compositions and an incomplete understanding of the transfer mechanism of the sediment-derived component to the mantle. In particular, with reference to the calculations presented in Fig. 15, the Ba/La ratios of added sediment melts should be lower than that of the bulk sediment because of the modal assemblage of the melting residue. In this case, the proportion of fluids in the added materials should increase.

7.3. Is there a slab window influence on the mantle source of the southernmost volcanoes of the SSVZ?

Cay, Maca, and Hudson are the three large central volcanoes of the SSVZ closest to the CTJ. Ridge subduction at the CTJ is the cause of the opening of a slab window to the SE that allows the subslab mantle to interact with the mantle wedge. Cenozoic basaltic magmas derived from the subslab mantle are widespread in extra-Andean Patagonia, and most show a typical within-plate geochemical signature (Stern et al., 1990; Gorring et al., 1997; D'Orazio et al., 2000; 2001). In the study region, lavas with within-plate affinity were found in the Río Murta area (Demant et al., 1998), ~30 km south of the Hudson volcano and close to the northern edge of the slab window.

The LILE/HFSE ratios of magmas from the Cay/Maca/Hudson region are as high as those commonly observed for magmas from convergent settings. For example, the average

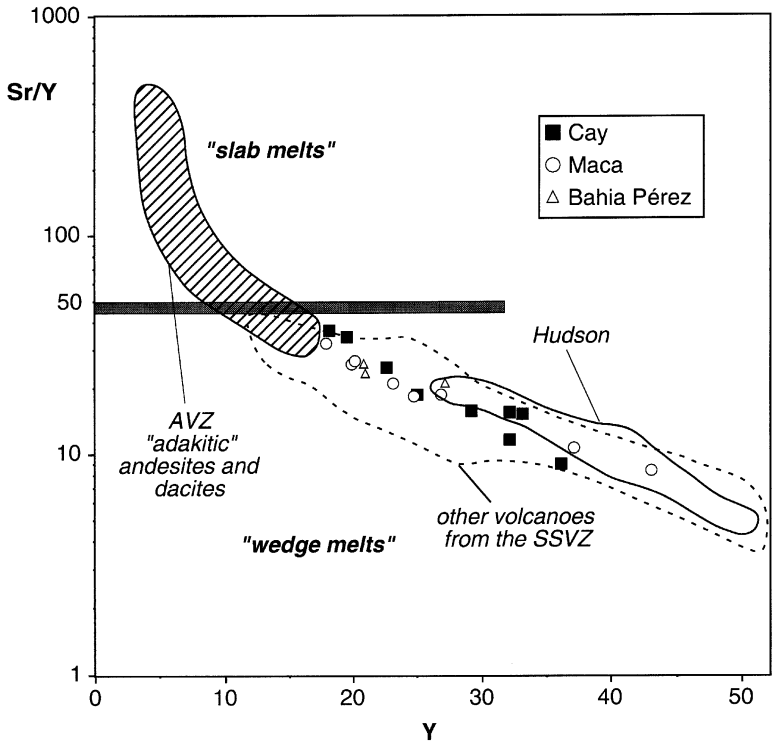

Fig. 14. Sr/Y versus Y (ppm) diagram for the SSUZ volcanics. The field for the AVZ adakitic rocks is also shown (Stern and Kilian, 1996). An Sr/Y ratio of approximately 50 is taken as the limit between slab melts and wedge melts (Yogodzinski et al., 2001). For the data sources, see Fig. 11; Lopez-Escobar et al. (1981).

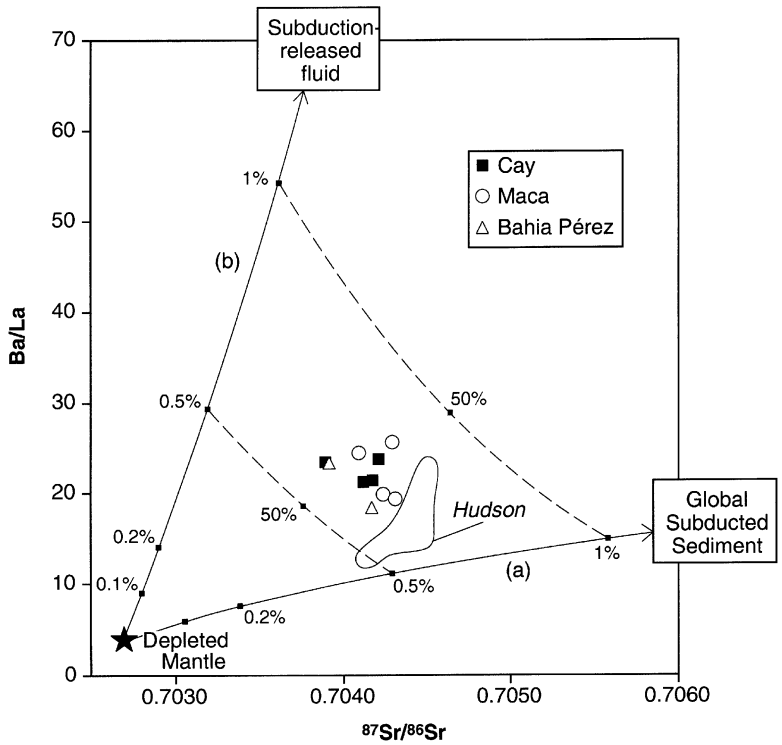

Fig. 15. Ba/La versus $^{87}Sr/^{86}Sr$ diagram. The bulk mixing curves between a depleted mantle source (Hofmann, 1988) and (a) the GLOSS (Plank and Langmuir, 1998) and (b) the estimated composition of the subduction-released fluid (Leeman et al., 1994) were also plotted. Numbers on the mixing lines refer to wt% of added subduction-derived material. The study samples fall in a region amid the curves, indicating that both slab-derived components were added to their sources. The results of the calculation suggest an input of subducted material to the preenrichment mantle < 1 wt%. Dashed lines were obtained by adding, to the depleted mantle, 0.5 and 1% of the subduction-derived mantle, made up of fluid and GLOSS in any proportion.

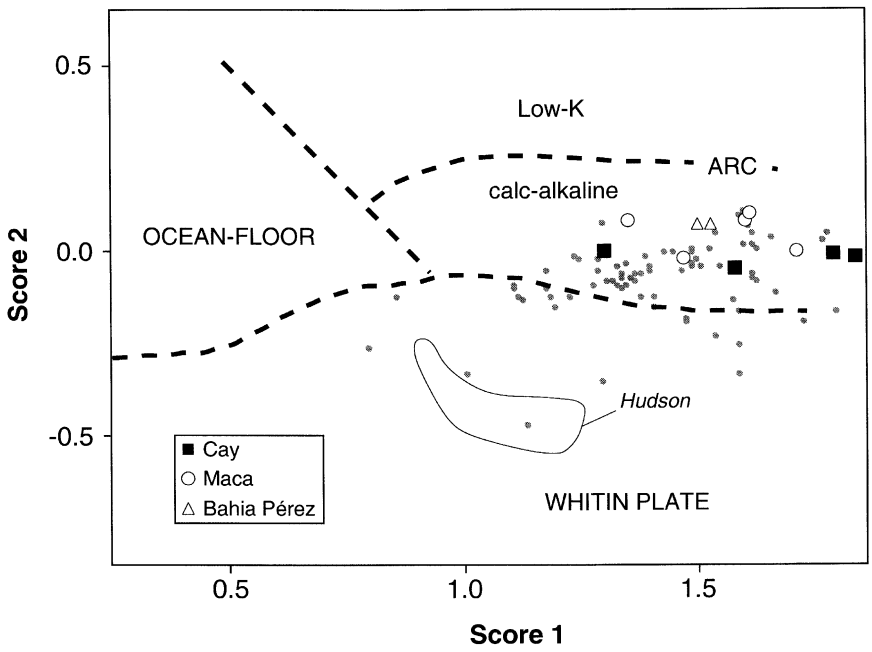

Fig. 16. Scores 1–2 discriminative diagram (Butler and Woronow, 1986). Basalts and basaltic andesites from the Cay and Maca volcanic regions plot within the field for typical calc-alkaline arc magmas, whereas the samples with the same degree of evolution from the Hudson volcano are distinct and fall in the field for within-plate magmas. The small dots are basalts and basaltic andesites from the SSVZ volcanoes north of Cay and Maca (see Fig. 11 for data sources). Scores 1 and 2 are complex function of the Ti, Sr, Zr, and Y whole-rock concentrations.

La/Nb ratio of the basalts and basaltic andesites from Cay/Maca/Bahia Pérez is 3.6 ± 0.3 (1 SD), which is indistinguishable from the average value of 3.5 ± 0.8 calculated for the same rock types in other calc-alkaline volcanoes of the SSVZ (Figs. 11 and 14). The Hudson volcanics show significantly lower La/Nb ratios (2.6 ± 0.2; Naranjo and Stern, 1998), and even lower ratios (~1.4) are observed for the Río Murta lavas (Demant et al., 1998). Because slab window-related Patagonian basalts have La/Nb ratios <1.2 (e.g. Stern et al., 1990; Gorring et al., 1997; D'Orazio et al., 2000), the progressive southward decrease of this ratio from Cay/Maca to Hudson to Río Murta could suggest the influence of the subslab mantle in the genesis of the Hudson magmas. This conclusion is supported by the mildly alkaline nature of the Hudson volcanics and their enrichment in HFSE (Fig. 9). A substantial difference in the mantle sources of the Cay/Maca and Hudson magmas is clearly shown in the discriminative diagram Scores 1–2 of Butler and Woronow (1986) (Fig. 16). In this diagram, according to the relative abundance of Ti, Zr, Sr, and Y, the basalts and basaltic andesites from Maca/Cay/Bahia Pérez fall in the field of typical calc-alkaline arc magmas, whereas basalts and basaltic andesites from the Hudson volcano plot in the field of within-plate basalts.

In summary, despite the relative closeness (~150 km) of the Cay and Maca volcanoes to the edge of the slab window generated by the ridge–trench collision, the geochemical features of the erupted magmas are typical of wedge melting, as observed along the SSVZ of the Andes. From the Cay and Maca volcanoes toward the slab window edge, we observe a reduction of the geochemical arc signature. As already stressed by Ramos and Kay (1992), magmas erupted by the Hudson volcano close to the slab window edge show a significant decrease in the LILE/HFSE ratios and an increase in alkalinity. We interpret this geochemical polarity as an effect of the incipient interaction, beneath the Hudson volcano, between the mantle wedge and the subslab mantle flowing through the slab window.

8. Conclusions

Cay and Maca are two large, neighboring stratovolcanoes located at the southern end of the SSVZ of the Andes. They rise in the southern portion of the Chiloe block at the intersection of NW–SE- and NE–SW-trending faults related to the LOFS. The erupted magmas display typical orogenic geochemical signatures, similar to those of the majority of the stratovolcanoes of the SSVZ. Volcanic rocks from the Cay and Maca regions form two roughly continuous and largely overlapping trends that range from medium-K subalkaline basalts to dacites. The Sr–Nd isotope compositions vary within a narrow range ($^{87}Sr/^{86}Sr = 0.70389–0.70431$ and $^{143}Nd/^{144}Nd = 0.51277–0.51284$) and overlap the most recurrent values observed for the SSVZ volcanics. Isotope and trace-element data suggest that crustal contamination made a minor contribution, if any, to the evolution of the magma studied, whereas the major- and trace-element variations combined with petrographical observations indicate the dominant

control of crystal fractionation (involving a gabbroic-removed solid) in magma evolution. The relative concentration of FME and fluid immobile elements in the Cay and Maca volcanics is compatible with the addition of small amounts (< 1 wt%) of both subducted sediments and slab-released fluids to their mantle sources. In spite of the very young age (< 10 Ma) of the oceanic lithosphere subducted beneath the Cay and Maca regions, there is no evidence for the involvement of slab melts in the genesis of the studied magmas. We compare the geochemistry of the Cay and Maca volcanics with that of volcanics from the Hudson volcano, which is located close to the northern edge of the slab window generated by the subduction of the Chile ridge segment. The existing data reveal that the magmatic products of the Cay and Maca volcanoes do not bear any geochemical imprint of the subslab asthenospheric mantle, whereas the lower LILE/HFSE ratios and higher alkalinity of the Hudson volcanics are ascribed to the influence of the subslab mantle rising through the nearby slab window.

Acknowledgements

We thank M. Delaloye and B. Déruelle for their review of the manuscript. This research was supported by PNRA and MURST (Italy), INACH/FONDEF Project MI-15 (Chile), and the International Cooperation C.N.R. (Italy)-CONYCIT (Chile).

Appendix A

Analytical methods

Mineral analyses were performed by a JEOL JXA-8600 electron microprobe (15 kV accelerating potential, 10 nA cup current, 2 μm beam spot), coupled with four WDS spectrometers, at the Centro di Studio per la Minerogenesi e Geochimica Applicata (C.N.R., Firenze), and by a Philips XL30 SEM equipped with an EDAX DX4 microanalytical system (20 kV accelerating potential, 10 nA beam current, 0.5 μm beam diameter) at the Dipartimento di Scienze della Terra, University of Pisa.

SiO_2, TiO_2, Al_2O_3, Fe_2O_{3tot}, MnO, MgO, CaO, Na_2O, K_2O, and P_2O_5 for the whole rocks were determined by XRF (ARL 9400 XP^+) on an $Li_2B_4O_7$ glass disk (sample:flux ratio 1:7) at the Dipartimento di Scienze della Terra, University of Pisa. FeO was determined by titration. Loss on ignition (LOI) was determined by gravimetry at 1000 °C after preheating at 110 °C. Estimated precisions for major-element data in the concentration ranges of the studied samples are better than 2%.

The concentrations of 31 trace elements were determined by ICP-MS (VG PQII Plus) at the Dipartimento di Scienze della Terra, University of Pisa. Samples were dissolved in PFA vessels on a hot plate at ~120 °C with HF + HNO_3. The sample solutions, at ca. 1:1000 dilution, were measured in replicates by external calibration. Analytical precisions, evaluated by repeated analyses of the in-house standard HE-1 (Mt. Etna hawaiite), are between 2 and 8% relative standard deviation.

Sr and Nd isotopic analyses were carried out using a Finnigan MAT 262V multicollector mass spectrometer at the Istituto di Geoscienze e Georisorse (C.N.R., Pisa) and conventional ion exchange methods for Sr and Nd separations. Measured $^{87}Sr/^{86}Sr$ ratios were normalized to $^{86}Sr/^{88}Sr = 0.1194$; $^{143}Nd/^{144}Nd$ ratios were normalized to $^{146}Nd/^{144}Nd = 0.7219$. During the collection of isotopic data for this study, replicate measurements of NIST SRM 987 ($SrCO_3$) and La Jolla standards gave values of 0.710226 ± 5 (2σ) for $^{87}Sr/^{86}Sr$ and 0.511852 ± 5 (2σ) for $^{143}Nd/^{144}Nd$. The measured $^{87}Sr/^{86}Sr$ and $^{143}Nd/^{144}Nd$ ratios for the samples of this study were normalized to a value of $^{87}Sr/^{86}Sr = 0.710250$ and $^{143}Nd/^{144}Nd = 0.511850$ for NIST SRM 987 and La Jolla, respectively.

References

Andersen, D.J., Lindsley, D.H., Davidson, P.M., 1993. QUILF: a PASCAL program to assess equilibria among Fe–Mg–Mn oxides, pyroxenes, olivine, and quartz. Computers and Geosciences 19 (9), 1333–1350.

Bach, W., Erzinger, J., Dosso, L., Bollinger, C., Bougault, H., Etoubleau, J., Sauerwein, J., 1996. Unusually large Nb–Ta depletions in North Chile Ridge basalts at 36°50′ to 38°56′S; major element, trace element, and isotopic data. Earth and Planetary Science Letters 142, 223–240.

Bourgois, J., Martin, H., Lagabrielle, Y., Le Moigne, J., Frutos Jara, J., 1996. Subduction erosion related to spreading-ridge subduction: Taitao peninsula (Chile margin triple junction area). Geology 24, 723–726.

Butler, J.C., Woronow, A., 1986. Discrimination among tectonic settings using trace element abundances of basalts. Journal of Geophysical Research 91 (B10), 10289–10300.

Cahill, T., Isacks, B.L., 1992. Seismicity and shape of the subducted Nazca plate. Journal of Geophysical Research 97, 17503–17529.

Cande, S.C., Leslie, R.B., 1986. Late Cenozoic tectonics of the Southern Chile Trench. Journal of Geophysical Research 91, 471–496.

Cembrano, J., Hervé, F., Lavenu, A., 1996. The Liquiñe–Ofqui fault zone: a long-lived intra-arc fault system in southern Chile. Tectonophysics 259, 55–66.

Demant, A., Belmar, M., Hervé, F., Pankhurst, R.J., Suárez, M., 1998. Pétrologie et géochimie des basaltes de Murta: une éruption sous-glaciaire dans les Andes patagoniennes (46° lat. S.), Chili. Relation avec la subduction de la ride du Chili. Comptes Rendus de l'Académie des Sciences Paris 327, 795–801.

Demant, A., Hervé, F., Pankhurst, R.J., Magnette, B., 1994. Alkaline and calc-alkaline Holocene basalts from minor volcanic centres in the Andes of Aysen, Southern Chile. VII Congreso Geológico Chileno, Actas II, 1326–1330.

DeMets, C., Gordon, R.G., Argus, D.F., Stein, S., 1994. Effect of recent revisions to the geomagnetic reversal time scale on estimate of current plate motions. Geophysical Research Letters 21 (20), 2191–2194.

Déruelle, B., Bourgois, J., 1991. Sur la dernière éruption du volcan Hudson (sud Chili, août 1991). Comptes Rendus de l'Académie des Sciences Paris 316, 1399–1405.

D'Orazio, M., Agostini, S., Mazzarini, F., Innocenti, F., Manetti, P., Haller, M.J., Lahsen, A., 2000. The Pali Aike volcanic field, Patagonia: slab-

window magmatism near the tip of South America. Tectonophysics 321, 407–427.

D'Orazio, M., Agostini, S., Innocenti, F., Manetti, P., Haller, M.J., Mazzarini, F., 2001. Slab window-related magmatism from southernmost South America: the Late Miocene mafic volcanics from the Estancia Glencross Area (~52°S, Argentina–Chile). Lithos 57, 67–89.

Forsythe, R.D., Nelson, E.P., 1985. Geological manifestations of ridge collision: Evidence from the Golfo de Penas-Taitao basin. Southern Chile. Tectonics 4 (5), 477–495.

Futa, K., Stern, C.R., 1988. Sr and Nd isotopic and trace element composition of Quaternary volcanic centers of southern Andes. Earth and Planetary Science Letters 88, 253–263.

Gerlach, D.C., Frey, F.A., Moreno-Roa, H., López-Escobar, L., 1988. Recent volcanism in the Puyehue–Cordon Caulle region, Southern Andes, Chile (40.5°S): petrogenesis of evolved lavas. Journal of Petrology 29, 333–382.

González-Ferrán, O., 1994. Volcanes de Chile, Instituto Geografico Militar, Santiago, 640 pp.

González-Ferrán, O., Innocenti, F., Lahsen, A., Manetti, P., Mazzuoli, R., Omarini, R., Tamponi, M., 1996. Alkali basalt volcanism along a subduction-related magmatic arc: the case of Puyuhuapi Quaternary volcanic line, Southern Andes (44°20′S), XIII Congreso Geológico Argentino y III Congreso de Exploracicen de Hidrocarburos, Buenos Aires, Actas III, pp. 549–565.

Gorring, M.L., Kay, S.M., 2001. Mantle processes and sources of Neogene slab window magmas from Southern Patagonia, Argentina. Journal of Petrology 42 (1), 1067–1094.

Gorring, M.L., Kay, S.M., Zeitler, P.K., Ramos, V.A., Rubiolo, D., Fernandez, M.I., Panza, J.L., 1997. Neogene Patagonian plateau lavas: Continental magmas associated with ridge collision at the Chile Triple Junction. Tectonics 16 (1), 1–17.

Guivel, C., Lagabrielle, Y., Bourgois, J., Maury, R.C., Fourcade, S., Martin, H., Arnaud, N., 1999. New geochemical constraints for the origin of ridge-subduction-related plutonic and volcanic suites from the Chile Triple Junction (Taitao Peninsula and Site 862, LEG ODP 141 on the Taitao Ridge). Tectonophysics 311, 83–111.

Herron, E.M., Cande, S.C., Hall, B.R., 1981. An active spreading center collides with a subduction zone, a geophysical survey of the Chile margin triple junction. Geological Society of America Memories 154, 683–701.

Hervé, F., Pankhurst, R.J., Drake, R., Beck, M.E., Mpodozis, C., 1993. Granite generation and rapid unroofing related to strike-slip faulting Aysen Chile. Earth and Planetary Science Letters 120, 375–386.

Hervé, F., Pankhurst, R.J., Drake, R., Beck, M.E., 1995. Pillow metabasalts in a Mid-Tertiary extensional basin adjacent to the Liquine–Ofqui fault zone: the Isla Magdalena area, Aysén, Chile. Journal of South American Earth Sciences 8 (1), 33–46.

Hickey, R., Frey, F.A., Gerlach, D., 1986. Multiple sources for basaltic arc rocks from the Southern Volcanic Zone of the Andes (34°–41°S): trace element and isotopic evidence for contributions from subducted oceanic crust, mantle, and continental crust. Journal of Geophysiscal Research 91 (B6), 5963–5983.

Hickey-Vargas, R., Moreno-Roa, H., López-Escobar, L., Frey, F.A., 1989. Geochemical variations in Andean basaltic and silicic lavas from the Villarrica–Lanin volcanic chain (39.5°S): an evaluation of source heterogeneity, fractional crystallization and crustal assimilation. Contributions to Mineralogy and Petrology 103, 361–386.

Hofmann, A.W., 1988. Chemical differentiation of the Earth: the relationship between mantle, continental crust, and oceanic crust. Earth and Planetary Science Letters 90, 297–314.

Housh, T.B., Luhr, J.F., 1991. Plagioclase-melt equilibria in hydrous systems. American Mineralogist 76, 477–492.

Klein, E.M., Karsten, J.L., 1995. Ocean-ridge basalts with convergent-margin geochemical affinities from the Chile Ridge. Nature 374, 52–57.

Lagabrielle, Y., Guivel, C., Maury, R.C., Bourgois, J., Fourcade, S., Martin, H., 2000. Magmatic–tectonic effects of high thermal regime at the site of active ridge subduction: The Chile Triple Junction model. Tectonophysics 326, 255–268.

Lahsen, A., López-Escobar, L., Vergara, M., 1994. The Puyuhuapi Volcanic Group, Southern Andes (44°20′S): geological and geochemical antecedents. VII Congreso Geológico Chileno, Actas II, 1076–1079.

Lahsen, A., González-Ferrán, O., Innocenti, F., Manetti, P., Mazzuoli, R., Omarini, R., Tamponi, M., 1997. New occurrence of orogenic volcanism along Liquiñe–Ofqui fault system: the Rio Pescado volcanic centers, Southern Andes (45°30′S, 73°04′W), Chile. VIII Congreso Geológico Chileno, Actas I, 108–112.

Leeman, W.P., Scheidegger, K.F., 1977. Olivine/liquid distribution coefficients and a test for crystal-liquid equilibrium. Earth and Planetary Science Letters 35, 247–257.

Leeman, W.P., Carr, M.J., Morris, J.D., 1994. Boron geochemistry of the Central America volcanic arc: constraints on the genesis of subduction-related magmas. Geochimica et Cosmochimica Acta 58, 149–168.

López-Escobar, L., Vergara, M., Frey, F.A., 1981. Petrology and geochemistry of lavas from Antuco volcano, a basaltic volcano of the Southern Andes (37°25′S). Journal of Volcanology and Geothermal Research 11, 329–352.

López-Escobar, L., Kilian, R., Kempton, P., Tagiri, M., 1993. Petrography and geochemistry of Quaternary rocks from the Southern Volcanic Zone of the Andes between 41°30′ and 46°00′S, Chile. Revista Geológica de Chile 20 (1), 33–55.

López-Escobar, L., Cembrano, J., Moreno, H., 1995a. Geochemistry and tectonics of the Chilean Southern Andes basaltic Quaternary volcanism (37–46°S). Revista Geológica de Chile 22 (2), 219–234.

López-Escobar, L., Parada, M.A., Hickey-Vargas, R., Frey, F.A., Kempton, P.D., Moreno, H., 1995b. Calbuco Volcano and minor eruptive centers distributed along the Liquiñe–Ofqui Fault Zone, Chile (41°–42°S): contrasting origin of andesitic and basaltic magma in the Southern Volcanic Zone of the Andes. Contributions to Mineralogy and Petrology 119, 345–361.

McDonough, W.F., Sun, S.S., 1995. The composition of the Earth. Chemical Geology 120, 223–253.

Miyashiro, A., 1974. Volcanic rock series in island arcs and active continental margins. American Journal of Science 274, 321–355.

Murdie, R.E., Russo, R.M., 1999. Seismic anisotropy in the region of the Chile margin triple junction. Journal of South American Earth Sciences 12, 261–270.

Naranjo, J.A., Stern, C.R., 1998. Holocene explosive activity of Hudson Volcano, southern Andes. Bulletin of Volcanology 59, 291–306.

Nelson, E., Forsythe, R., Arit, I., 1994. Ridge collision tectonics in terrane development. Journal of South American Earth Sciences 7, 271–278.

Parada, M.A., Lahsen, A., Palacios, C., 2000. The Miocene plutonic event of the Patagonian Batholith at 44°30′S: thermochronological and geobarometric evidence for melting of a rapidly exhumed lower crust. Transactions of the Royal Society of Edinburgh: Earth Sciences 91, 169–179.

Peacock, S.M., Rushmer, T., Thompson, A.L., 1994. Partial melting of subducted oceanic crust. Earth and Planetary Science Letters 121, 227–244.

Peccerillo, A., Taylor, S.R., 1976. Geochemistry of Eocene calc-alkaline volcanic rocks from the Kastamonu Area, northern Turkey. Contribution to Mineralogy and Petrology 58, 63–81.

Plank, T., Langmuir, C.H., 1998. The chemical composition of subducting sediment and its consequences for the crust and mantle. Chemical Geology 145, 325–394.

Ramos, V.A., Kay, S.M., 1992. Southern Patagonian plateau basalts and deformation: Backarc testimony of ridge collisions. Tectonophysics 205, 261–282.

Sack, R.O., Ghiorso, M.S., 1991. Chromian spinels as petrogenetic indicators; thermodynamics and petrological applications. American Mineralogist 76, 827–847.

Sigmarsson, O., Martin, H., Knowles, J., 1998. Melting of a subducting oceanic crust from U–Th disequilibria in Austral Andean lavas. Nature 394, 566–569.

Stern, C.R., Kilian, R., 1996. Role of the subducted slab, mantle wedge and continental crust in the generation of adakites from the Andean Austral Volcanic Zone. Contribution to Mineralogy and Petrology 123, 263–281.

Stern, C.R., Frey, F.A., Futa, K., Zartman, R.E., Peng, Z., Kyser, T.K., 1990. Trace-element and Sr, Nd, Pb and O isotopic composition of Pliocene and Quaternary alkali basalt of the Patagonian Plateau lavas of southernmost South America. Contribution to Mineralogy and Petrology 104, 294–308.

Taylor, S.R., McLennan, S.M., 1985. The Continental Crust: Its Composition and Evolution, Blackwell Scientific Publication, Oxford, 312 pp.

Tebbens, S.F., Cande, S.C., Kovacs, L., Parra, J.C., LaBrecque, J.L., Vergara, H., 1997. The Chile ridge: a tectonic framework. Journal of Geophysical Research 102, 12035–12059.

Yogodzinski, G.M., Lees, J.M., Churikova, T.G., Dorendorf, F., Wörner, G., Volynets, O.N., 2001. Geochemical evidence for the melting of subducting oceanic lithosphere at plate edges. Nature 409, 500–503.